Free Radical Biology and Medicine 253 (2026) 527–543

Contents lists available at ScienceDirect

Free Radical Biology and Medicine

journal homepage: www.elsevier.com/locate/freeradbiomed

Probiotic-driven gut–liver redox crosstalk modulates hepatic Nrf2 signaling pathway and attenuates metabolic dysfunction-associated steatohepatitis

Da Hyun Lee [a,1], Da Ye Kim [a,b,1], Hyunchae Joung [c,1], Hyolim Kim [d], Yujin Jeon [d], Sunghee Lee [c], Chang Hun Shin [c], Yu Seol Lee [a,b], Ji Yun Bang [a,b], Eo Jin Lee [a,b], Shin Young Cha [a], Soo Han Bae [a,b,*], Hye Won Lee [d,e,**]

[a] Department of Biomedical Sciences, Yonsei University College of Medicine, Seoul, 03722, Republic of Korea
[b] Department of Biomedical Sciences, Graduate School of Medical Science, Brain Korea 21 Project, Yonsei University College of Medicine, Seoul, 03722, Republic of Korea
[c] Central Research Institute, Chong Kun Dang Bio, Ansan, 15604, Republic of Korea
[d] Department of Internal Medicine, Institute of Gastroenterology, Yonsei University College of Medicine, Seoul, 03722, Republic of Korea
[e] Yonsei Human Microbiome Center, Yonsei University College of Medicine, Seoul, 03722, Republic of Korea

ARTICLE INFO

Keywords:
MASH
Gut–liver axis
Gut microbiome
Nrf2
Glutathione
ROS
Probiotics

ABSTRACT

Metabolic dysfunction-associated steatohepatitis (MASH) is a chronic liver disease characterized by persistent inflammation, oxidative stress, and progressive fibrosis. There is currently no effective pharmacological therapy for MASH. We investigated whether two defined probiotic bacteria strains, *Lactobacillus delbrueckii* subsp. *lactis* (*L. lactis*) CKDB001 and *Lactiplantibacillus plantarum* (*L. plantarum*) Q180, attenuate MASH pathology in association with modulation of gut-liver redox signaling. Using diet-induced preventive and therapeutic mouse models of MASH, we showed that oral administration of these strains significantly improved hepatic steatosis, robustly attenuates fibrosis, and reduced inflammatory and oxidative stress markers. Probiotic treatment was associated with increased intestinal glutathione availability, and was accompanied by activation of hepatic nuclear factor erythroid 2-related factor 2 (Nrf2) signaling and upregulation of canonical antioxidant enzymes, consistent with improved hepatic redox homeostasis and reduced hepatocellular injury. Microbiome profiling revealed successful intestinal persistence of the administered strains and enrichment of other bacterial taxa associated with gut barrier integrity and metabolic resilience, including *Akkermansia muciniphila*, *Parabacteroides goldsteinii*, and *Mediterraneibacter butyricigenes*. Functional prediction analysis further suggested enhancement of microbial glutathione metabolism pathways, supporting a potential role for microbiota-driven redox modulation in host protection. Therapeutic efficacy was maintained after disease establishment and under conditions recapitulating features of a lean MASH-like phenotype, highlighting obesity-independent mechanisms of action. Collectively, our findings support a probiotic-driven association between intestinal glutathione dynamics and hepatic Nrf2 activation within the gut-liver axis, providing a mechanistically informed and translationally relevant framework for MASH intervention.

1. Introduction

Metabolic dysfunction-associated steatohepatitis (MASH), formerly known as nonalcoholic steatohepatitis, is a severe and progressive form of fatty liver disease characterized by excessive hepatic lipid accumulation, oxidative stress, and inflammation [1,2]. Lipotoxicity-induced mitochondrial dysfunction and reactive oxygen species (ROS) overproduction play pivotal roles in hepatocellular injury and fibrogenesis, amplifying the inflammatory cascade that drives disease progression [3–5]. Although lifestyle modifications such as dietary

* Corresponding author. Department of Biomedical Sciences, Yonsei University College of Medicine, 50-1 Yonsei-ro, Seodaemun-gu, Seoul, 03722, Republic of Korea.
** Corresponding author. Department of Internal Medicine, Yonsei University College of Medicine, 50-1 Yonsei-ro, Seodaemun-gu, Seoul, 03722, Republic of Korea.
E-mail addresses: soohanbae@yuhs.ac (S.H. Bae), LORRY-LEE@yuhs.ac (H.W. Lee).
[1] These authors contributed equally to this work.

https://doi.org/10.1016/j.freeradbiomed.2026.05.338
Received 10 February 2026; Received in revised form 21 May 2026; Accepted 30 May 2026
Available online 1 June 2026

control, physical activity, and weight reduction remain the current first-line therapies for MASH [6], their long-term adherence and clinical sustainability are limited.

A substantial proportion of patients develop MASH in the absence of obesity, a condition referred to as "lean MASH," which is increasingly recognized worldwide [7]. Lean MASH patients often exhibit severe hepatic inflammation and fibrosis despite a normal body mass index, and they respond poorly to weight loss-based interventions, underscoring the involvement of non-adiposity-driven pathogenic mechanisms such as oxidative stress and gut-derived metabolic disturbances [8]. Recently, resmetirom and semaglutide have shown clinical benefits and gained approval for MASH management, yet significant limitations remain regarding their efficacy, accessibility, and long-term outcomes [9,10]. This underscores the urgent need for novel, safe, and mechanistically grounded therapeutic approaches.

Accumulating evidence implicates the gut–liver axis as a central modulator of MASH pathogenesis [11]. Dysbiosis, characterized by decreased microbial diversity, gram-negative bacterial overgrowth, and altered microbial metabolites in the intestine, contributes to metabolic inflammation and hepatic injury due to increased gut permeability and endotoxin translocation [12,13]. Beyond immune and metabolic signaling, emerging studies highlight the significance of intestinal redox imbalance as a key upstream driver of hepatic oxidative stress [14]. Perturbations of gut antioxidant capacity may contribute to systemic ROS elevation and disrupt hepatic redox homeostasis, thereby aggravating lipid peroxidation and fibrogenic signaling.

Among the endogenous antioxidant systems, nuclear factor erythroid 2-related factor 2 (Nrf2) serves as a master transcriptional regulator that maintains cellular redox balance. Nrf2 orchestrates the expression of detoxifying enzymes such as NAD(P)H quinone oxidoreductase 1 (NQO1), glutathione S-transferases (GSTs), and heme oxygenase-1 (HO-1), thereby limiting oxidative injury [15]. Impaired Nrf2 signaling has been consistently observed in MASH, resulting in diminished antioxidant defenses [16]. Enhancement of Nrf2-associated antioxidant responses thus represents a promising strategy for alleviating redox-driven liver injury. Notably, both genetic and pharmacological studies have demonstrated that Nrf2 plays a protective role against steatohepatitis and liver injury [17,18]. Intriguingly, recent findings indicate that gut-derived metabolites, including glutathione (GSH), have been implicated in the regulation of hepatic redox signaling and systemic redox status [19]. Because the intestine contributes significantly to systemic GSH biosynthesis, maintenance of intestinal GSH pools may play an important role in sustaining hepatic antioxidant capacity [20].

Probiotic-based interventions have emerged as attractive candidates for rebalancing the gut–liver axis because of their multi-layered biological effects, including modulation of gut microbial composition, intestinal barrier integrity, and metabolic signaling [21]. Specific strains within the *Lactobacillus* genera possess intrinsic antioxidant potential and are capable of stimulating host GSH synthesis and scavenging free radicals [22,23]. However, the mechanistic link between probiotic-driven intestinal redox enhancement and hepatic antioxidant responses remains poorly defined.

In the present study, we investigated the therapeutic potential of two probiotic strains, *Lactobacillus delbrueckii* subsp. *lactis* (*L. lactis*) CKDB001 and *Lactiplantibacillus plantarum* (*L. plantarum*) Q180, in attenuating MASH progression by modulating the gut–liver redox axis. Using diet-induced mouse models recapitulating key features of lean MASH, we demonstrate that oral administration of these probiotic strains significantly alleviates hepatic steatosis, inflammation, and fibrosis. We observed a robust increase in intestinal GSH levels following probiotic treatment, which was associated with enhanced hepatic Nrf2-related antioxidant responses and upregulation of downstream antioxidant enzymes. Our findings delineate a potential gut-derived redox communication, whereby probiotic-induced intestinal GSH elevation is associated with enhanced hepatic NRF2 signaling and reduced oxidative stress and liver injury. These findings support *L. lactis* CKDB001 and *L. plantarum* Q180 as promising microbiome-based therapeutic candidates for restoring redox homeostasis in MASH.

2. Material and methods

2.1. Animals and experimental MASH

All animal experiments were approved by the Animal Care and Use Committee of the Yonsei University College of Medicine (**IACUC: 2023–0164**). Male C57BL/6J mice (Japan SLC, Inc., SLC-M-0133) aged 7 weeks were used in all animal experiments to minimize potential variability associated with sex-dependent differences in MASH progression and redox responses. A one-week acclimation period was provided. All mice had free access to water and food and were housed in cages maintained at $23 \pm 2\,^{\circ}C$ under a 12 h light/12 h dark cycle and 50%-70% humidity. Mice were assigned to three groups: mice fed a normal chow diet (NC; LabDiet, 5053) for non-treated wild type, mice fed a high-fat, high cholesterol diet (Dyets 600024; Purina #5015 Mouse Chow with 27.5% Palm Oil, 2.5% Cholesterol, & 2% Cholic Acid) with 2.3% fructose water (Sigma F0127) for MASH development, and MASH mice treated with *L. lactis* CKDB001 or *L. plantarum* Q180. For the prevention model, mice received oral gavage of each strain five times per week for 8 weeks at 1.0×10^9 CFU/day. For the therapeutic model, MASH was induced by feeding mice a MASH diet for 4 weeks, followed by oral gavage of each strain five times per week for an additional 4 weeks at either a low dose (L; 1.0×10^9 CFU/day) or a high dose (H; 5.0×10^9 CFU/day). All experimental mice in this study were reared under humane conditions and monitored weekly for weights.

2.2. Preparation of probiotic strain

L. lactis CKDB001 and *L. plantarum* Q180 were prepared as previously described, with minor modifications [24,25]. Briefly, each strain was cultured in optimized media under strain-specific optimal growth conditions until reaching the late exponential phase. Bacterial cells were harvested by centrifugation and lyophilized under the appropriate conditions. The viable cell count was determined based on colony-forming units (CFU) before administration. Mice were orally administered either a low dose (1.0×10^9 CFU/day) or a high dose (5.0×10^9 CFU/day) of each probiotic strain by gavage for the indicated treatment period. Fresh bacterial suspensions were prepared daily to ensure viability and consistency of dosing.

2.3. Analysis of gut environment based upon 16s rRNA sequencing

At the end of the treatment period, fecal samples were collected aseptically, immediately snap-frozen in liquid nitrogen, and stored at −80 °C until analysis. Microbial genomic DNA was extracted using the QIAamp® DNA Stool Mini Kit (QIAGEN, Hilden, Germany) according to the manufacturer's instructions. The V3–V4 hypervariable regions of the bacterial 16S rRNA gene were amplified using region-specific primers, and purified amplicons were sequenced on an Illumina MiSeq platform (Illumina Inc., San Diego, CA, USA). Raw sequencing reads were processed using the QIIME2 pipeline. Quality filtering, denoising, paired-end read merging, chimera removal, and feature table construction were performed using the DADA2 plugin. Alpha diversity was evaluated using the Chao1 index, while beta diversity was assessed by principal coordinate analysis (PCoA) based on Bray–Curtis. Taxonomic classification was performed using the NCBI and SILVA reference databases. Species-level annotation was conducted via local BLASTN (ncbi-blast-2.10.0+) against the NCBI RefSeq 16S rRNA database (updated February 11, 2020), and representative sequences were additionally classified using the SILVA v138 99% full-length 16S rRNA database. Microbial composition was analyzed at the phylum level. Differentially abundant taxa between groups were identified using linear discriminant analysis effect size (LEfSe). Functional pathway prediction was

conducted using PICRUSt2 based on 16S rRNA gene profiles. All sequencing procedures and bioinformatic analyses, including DNA extraction and library preparation, were performed by 3BIGS Co., Ltd. (Hwaseong, Republic of Korea).

2.4. Histological and immunohistochemical analysis

The livers of mice were fixed in 10% formalin solution (Sigma-Aldrich, HT501128). Ileum tissues were rolled, fixed in 10% formalin solution for 24 h, incubated in 30% sucrose, re-fixed in 10% formalin solution, and embedded in paraffin. Paraffin-embedded tissues were sectioned at a thickness of 5 μm. Paraffin liver sections were stained with hematoxylin and eosin (H&E), Masson's trichrome (MTS), and Sirius red, or subjected to immunohistochemical analysis using antibodies against 4-hydroxynonenal (4-HNE; Jaica MHN-D20P), 3-nitrotyrosine (3-NT; Millipore, 06-284), and Nrf2 (Invitrogen, PA5-27882). Paraffin ileum sections were immunostained for occludin (OCLN; Cell Signaling Technology, 91131). Histological scoring was performed in a blinded manner by independent investigators. Collagen-positive areas in Sirius red- and Masson's trichrome-stained liver sections were manually evaluated by microscopic examination in a blinded manner and expressed as the percentage of stained area.

2.5. Measurement of superoxide levels by DHE staining

Intracellular superoxide production was assessed using dihydroethidium (DHE; D11347). Cryosections of liver tissue (5 μm thick) were fixed in acetone at −20 °C for 10 min, air-dried, and incubated with 20 μM DHE for 45 min at 37 °C in the dark. Sections were then mounted with Fluoroshield with DAPI (Sigma-Aldrich, F6057) and incubated overnight. Images were acquired using a confocal microscope (Carl Zeiss, LSM 780). The relative fluorescence intensity was quantified by averaging fluorescence signals from randomly selected fields per section after subtraction of background fluorescence using ImageJ (NIH).

2.6. Terminal deoxynucleotidyl transferase-mediated dUTP nick-end labeling (TUNEL) analysis

To evaluate apoptosis in mouse livers, a TUNEL assay kit (Promega, G3250) was used according to the manufacturer's instructions. Paraffin-embedded liver sections were deparaffinized and permeabilized by incubation with proteinase K solution (20 μg/mL) for approximately 10 min at room temperature. After washing, sections were re-fixed in formalin for 5 min and incubated with 100 μL of equilibration buffer per slide for 10 min at room temperature. For labeling, 50 μL of TdT reaction mix was applied to each slide, covered with plastic coverslips, and incubated at 37 °C for 1 h in the dark. The reaction was stopped by incubation with 2× SSC for 15 min, followed by washing. All washing steps during the TUNEL assay were performed using 1× dulbecco phosphate buffered saline (DPBS). Sections were mounted with Fluoroshield with DAPI and coverslipped. Fluorescence signals were detected using a confocal microscope (Carl Zeiss, LSM 780). Apoptosis was quantified by calculating the percentage of TUNEL-positive cells in three randomly selected microscopic fields.

2.7. Immunoblot analysis

For immunoblot analysis, the liver tissues were homogenized in lysis buffer containing 20 mM HEPES-KOH (pH 8.0), 150 mM NaCl, 1 mM EDTA, 1% Nonidet P-40 (NP-40), 0.3% Triton X-100, 10% glycerol, 1 mM Na_3VO_4, 5 mM NaF, and protease inhibitors (aprotinin and leupeptin). The liver lysates were centrifuged (13,500 rpm for 15 min), and the resulting supernatants were subjected to sodium dodecyl sulfate polyacrylamide gel electrophoresis (SDS-PAGE); the separated proteins were transferred to polyvinylidene fluoride membranes (PVDF; Millipore, IPVH00010). After blocking with 5% skim milk in Tris-buffered saline and 0.1% Tween 20 (TBS-T) for 30 min, the membranes were then incubated with the specific primary antibodies at 4 °C overnight. The membranes were then incubated with horseradish peroxidase-conjugated secondary antibodies at room temperature for 1 h. The proteins were visualized using an enhanced chemiluminescence solution (Thermo Scientific, 34580). Densitometric analysis of protein bands was performed using Fiji/ImageJ software (NIH). The following antibodies were used to detect the target proteins: anti-COL1A1 (Cell Signaling Technology, 72026); anti-αSMA (Abcam, ab5694); anti-GAPDH (Santa Cruz Biotechnology, SC-25778); anti-Fibronectin (Abcam, ab2413); anti-p-IkBα (Ser32) (Cell Signaling Technology, 2859); anti-IkBα (Cell Signaling Technology, 9242); anti-Occludin (Abcam, ab167161); anti-β-actin (Santa Cruz Biotechnology, sc-47778); anti-Nrf2 (Proteintech, 16396-1-AP); anti-Lamin B1 (Proteintech, 12987-1-AP); anti-HO-1 (Santa Cruz Biotechnology, sc-136960); anti-NQO1 (Santa Cruz Biotechnology, sc-32793); anti-α-tubulin (Santa Cruz Biotechnology, sc-5286).

2.8. Measurement of pro-inflammatory cytokines and LPS by ELISA

The levels of pro-inflammatory cytokines in liver tissue were detected using commercial ELISA kits (TNFα, R&D Systems, MTA00B; IL-6, R&D Systems, M6000B) according to the manufacturers' instructions. Lipopolysaccharide (LPS) levels were measured separately in serum and stool samples using a commercial ELISA kit (Aviva Systems Biology, OKEH02594). For serum LPS measurement, blood samples were collected and centrifuged to obtain serum. For stool LPS measurement, fecal samples were homogenized in endotoxin-free buffer and centrifuged, and the supernatant was used for analysis. Optical density was measured at 450 nm using a microplate reader (Molecular Devices, VersaMax).

2.9. Analysis of hepatic mRNAs using quantitative RT-PCR

Total RNA (1 μg) was extracted using TRIzol Reagent (Invitrogen, 15596018) and reverse-transcribed into cDNA with a cDNA synthesis kit (Takara, RR036A). Quantitative PCR was conducted using SYBR® Green (ABI, 4367659) on a QuantStudio 3 (Applied Biosystems) with the mouse-specific primer pairs (forward and reverse). For qPCR analysis, RNA was extracted from pooled samples within each experimental replicate. Although experiments were performed independently, pooling precluded visualization of individual sample dots. The PCR reaction was initiated by heating at 55 °C for 2 min and at 95 °C for 10 min, followed by 40 amplification cycles with denaturation at 95 °C for 15 s, annealing and extension at 60 °C for 1 min. The expression of specific genes was quantified by the $2-\Delta\Delta Ct$ (delta-delta Ct) method. The mRNA expression levels of each gene were normalized to those of 18S mRNA, which was a housekeeping gene and not altered by our interventions.

- Mouse-specific primer pairs (forward and reverse) used for cDNA were as follows:

Acta2, 5′-CTGACAGAGGCACCACTGAA-3′ and 5′-CATCTCCAGAGT CCAGCACA-3’; *Tgfβ*, 5′-TTGCTTCAGCTCCACAGAGA-3′ and 5′-TGGTTG TAGAGGGCCAAGGAC-3’; *Col1a1*, 5′-GAGCGGAGAGTACTGGATCG-3′ and 5′-GCTTCTTTTCCTTGGGGTTC-3’; *Col3a1*, 5′-TGTTCAGCTTTGTG-GACCTC-3′ and 5′-TCAAGCATACCTCGGGTTTC-3’; *Gsta1*, 5′-TGCC CAATCATTTCAGTCAG-3′ and 5′-CCAGAGCCATTCTCAACTA-3’; *Nqo1*, 5′-TTCTCTGGCCGATTCAGAG-3′ and 5′-GGCTGCTTGGAGCAAAATAG-3’; *Ho-1*, 5′-GAGCAGAACCAGCCTGAACTA-3′ and 5′- GGTACAAGGAAG CCATCACCA-3’; *Adgre1*, 5′-CTTTGGCTATGGGCTTCCAGT-3′ and 5′-GCAAGGAGGACAGAGTTTATCGTG-3’; *Il-1β*, 5′-AACCTGCTGGTGTGT-GACGTTC-3′ and 5′-CAGCACGAGGCTTTTTTGTTGT-3’; *Ccl2*, 5′-TCTCT CTTCCTCCACCACCATG-3′ and 5′-GCGTTAACTGCATCTGGCTGA-3’;

Tnfα, 5′-GCCTCTTCTCATTCCTGCTTG-3′ and 5′-CTGATGAGAGGGAGG CCATT-3’; 18S, 5′-CGCTCCCAAGATCCAACTAC-3′ and 5′-CTGAGAAA CGGCTACCACATC-3’.

2.10. Analysis of serum biochemical parameters

Blood samples were obtained from cardiac puncture of mice. Serum was separated by centrifuging at 3000 rpm for 10 min. The serum samples were stored at −80 °C for further use. Serum alanine aminotransferase (ALT; 3250), aspartate aminotransferase (AST; 3150), alkaline phosphatase (ALP; 3550), total cholesterol (TCHO; 1450), high-density lipoprotein cholesterol (HDL-C; 2650), and triglyceride (TG; 1650) levels were measured via colorimetric determination using an activity assay kit (Fujifilm, Tokyo, Japan) according to the manufacturer's instructions.

2.11. Lipid accumulation measurement in the liver

For Oil Red O (ORO) staining, a 0.7% Oil Red O solution was prepared by dissolving Oil Red O powder (Sigma-Aldrich, O0625) in propylene glycol (Duksan Pure Chemicals, 57-55-6), followed by incubation in a 60 °C water bath with agitation overnight. The solution was filtered two to three times before use. Frozen liver tissues were embedded in OCT compound in cryomolds and stored at −80 °C. Frozen sections (5 μm thick) were prepared using a cryostat. Cryosections were air-dried, fixed in 10% formalin, dehydrated with propylene glycol, and stained with Oil Red O solution for approximately 10 min at 60 °C. Nuclei were counterstained for 1 min at room temperature. Hepatic triglyceride content was quantified using a triglyceride colorimetric assay kit (Cayman Chemical, ETGA-200) according to the manufacturer's instructions.

2.12. Measurement of hepatic hydroxyproline content

Liver tissues (20 mg) were hydrolyzed in 200 μL of 12 N HCl in Teflon-sealed pressure vials at 120 °C for 3 h. After hydrolysis, aliquots of the samples (10 μL) were dried at 65 °C in a 96-well plate. Hydroxyproline levels were then quantified using a hydroxyproline colorimetric assay kit (Abcam, ab222941) according to the manufacturer's instructions for the colorimetric detection step.

2.13. Statistical analysis

Data were analyzed using two-tailed Student's t-tests for comparisons between two groups or one-way analysis of variance (ANOVA) followed by Tukey's post hoc test for multiple-group comparisons. Statistical analyses were performed using GraphPad Prism 10 (GraphPad Software, La Jolla, CA, USA), and a P value < 0.05 was considered statistically significant. Correlation analysis between species-level microbial relative abundance and predicted functional pathway abundance was performed using Pearson's correlation coefficients to assess the associations between microbial composition and functional potential.

2.14. Nuclear fractionation

Nuclear and cytoplasmic fractions were prepared using cytoplasmic and nuclear extraction reagents according to the manufacturer's protocol. Mouse liver tissues were first homogenized in cytoplasmic extraction buffer composed of 10 mM HEPES (bioWORLD, 40820042-1), 1.5 mM $MgCl_2$, 10 mM KCl, 0.05% IGEPAL® CA-630 (Sigma Aldrich, 56741), 0.5 mM dithiothreitol (DTT) (Sigma Aldrich, 10197777001), 2 mM PMSF (Sigma Aldrich, 10837091001), 1 mg/mL aprotinin (Sigma Aldrich, A3428), and 1 mg/mL leupeptin (Sigma Aldrich, L2884). The homogenates were centrifuged at 3000 rpm for 10 min to separate the cytoplasmic fraction. The resulting pellets were then resuspended in nuclear extraction buffer containing 5 mM HEPES (pH 8.0), 1.5 mM $MgCl_2$, 0.2 mM EDTA, 26% glycerol, and 0.5 mM DTT. Subsequently, NaCl was added to the suspension (final concentration, 300 mM) to facilitate efficient lysis, followed by incubation on ice. Subsequently, the samples were centrifuged at 15,000 rpm for 30 min, and the collected supernatants were used as nuclear extracts. Protein levels of Nrf2 and Lamin B1 (a nuclear protein marker) were analyzed by immunoblotting as described previously [26,27]. Protein concentrations in each fraction were determined using the Bradford protein assay.

2.15. Measurement of glutathione and GSH/GSSG ratio

Glutathione levels in cecal contents and liver tissues were measured using a commercially available enzymatic assay kit (EnzyChrom™ GSH/GSSG Assay Kit, BioAssay Systems, EGTT-100) according to the manufacturer's instructions. Cecal contents and liver tissues were immediately homogenized in cold phosphate buffer (50 mM, pH 7.0) containing 1 mM EDTA to minimize thiol oxidation during sample preparation. All sample preparation procedures were performed on ice, and sample were processed immediately after collection. For GSSG measurement, scavenger reagent provided in the assay kit was added to mask reduced glutathione (GSH). Samples were centrifuged at 10,000 × g for 5 min at 4 °C, and the resulting supernatants were collected for further analysis. For total glutathione measurement, samples without scavenger reagent were centrifuged at 10,000 × g for 15 min at 4 °C prior to supernatant collection. Glutathione levels were determined using an enzymatic recycling method in which 5,5′-dithiobis-(2-nitrobenzoic acid) (DTNB) reacts with GSH, coupled with glutathione reductase and NADPH, and absorbance was measured at 412 nm using a microplate reader. The assay was performed according to the manufacturer's validated protocol designed to minimize interference from non-glutathione thiols. Total glutathione and GSSG concentrations were calculated from standard curves, and reduced GSH levels were determined by subtracting twice the GSSG value from total glutathione. The GSH/GSSG ratio was calculated as an indicator of redox balance.

3. Results

3.1. Probiotic treatment reduces hepatic steatosis and inflammation in a MASH preventive model

To evaluate the effects of *L. lactis* CKDB001 and *L. plantarum* Q180 on MASH progression, we established a MASH preventive model in eight-week-old male C57BL/6 mice. Following a one-week oral adaptation period, mice were assigned to four experimental groups. The normal chow diet (NC) group received standard chow and a phosphate-buffered saline (PBS) vehicle, whereas the remaining groups were fed a MASH diet (high-fat, high-cholesterol diet with high-fructose drinking water). Among the three MASH groups, mice received either PBS (vehicle; Veh), *L. lactis* CKDB001, or *L. plantarum* Q180 via oral administration five times per week starting at the initiation of MASH diet feeding and continuing for 8 weeks (Fig. 1A). Body weight was monitored weekly throughout the experimental period (Fig. S1A). Liver weight was significantly increased in all MASH groups compared with the NC group, and a similar increase was observed in the liver-to-body weight ratio (Fig. 1B). Gross liver morphology further demonstrated a clear phenotypic distinction between the NC and MASH groups; however, no overt macroscopic differences were observed between the mice treated with *L. lactis* CKDB001 and those treated with *L. plantarum* Q180 (Fig. S1B).

The MASH diet used in this study recapitulated features of a lean MASH model, as evidenced by a marked reduction in adipose tissue mass. Accordingly, the weights of epididymal white adipose tissue (eWAT) and subcutaneous white adipose tissue (sWAT) were significantly decreased in all MASH groups compared with the NC group (Fig. S4A–B), with no significant differences observed between the microbial treatment groups (Fig. S1C). In addition, glucose tolerance was not markedly impaired (Fig. S4C), suggesting relatively preserved

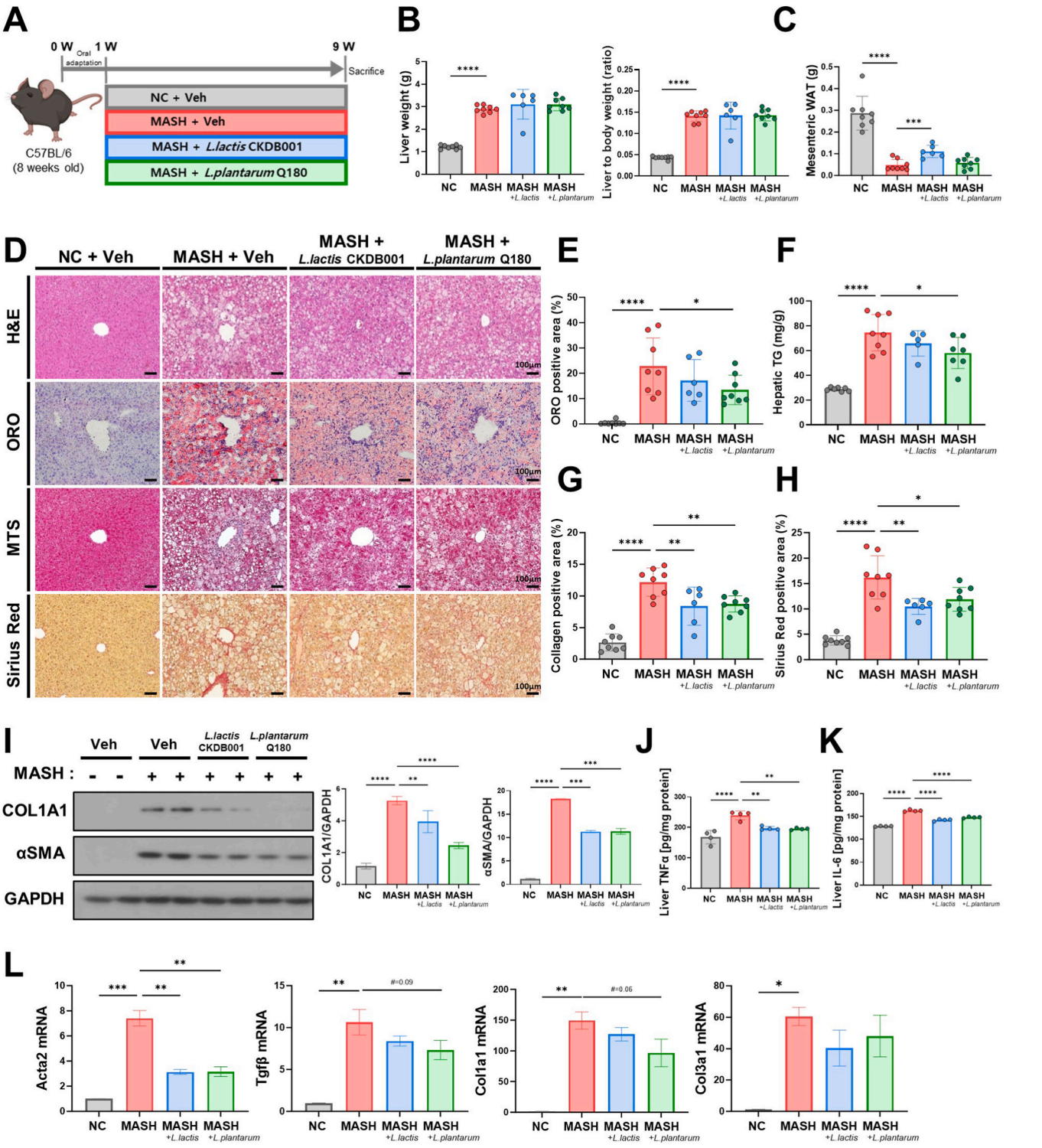

Fig. 1. Protective Effects of *L. lactis* CKDB001 and *L. plantarum* Q180 Against Lipid Accumulation, Inflammation, and Fibrosis in a MASH Prevention Model.

Experimental scheme: 8-week-old B6 mice were acclimated for one week and then fed either a normal chow diet (NC) or a high-fat, high-cholesterol, high-fructose (HFHCF) diet for eight weeks, with the latter defined as the MASH group. During the feeding period, bacterial strains were administered orally five times per week (A). Liver weight (g) and liver-to-body weight (B.W.) ratio (B), mesenteric white adipose tissue (WAT) weight (g) (C), representative liver sections stained with H&E, Oil Red O, Masson's trichrome (MTS), and Sirius Red, scale bars 100 μm (D), quantification of Oil Red O positive area (%) (E), hepatic triglyceride (TG) content (mg/g liver) (F), quantification of collagen area (%) and Sirius red collagen area (%) (G, H), immunoblot analysis of COL1A1 and αSMA in liver lysates with GAPDH as a loading control and quantification of protein levels (I), hepatic TNFα content (pg/mg protein) (J), hepatic IL-6 content (pg/mg protein) (K), and hepatic mRNA levels of *Acta2, Tgfβ, Col1a1,* and *Col3a1* (L). Each data point represents an individual mouse (biological replicate), unless otherwise indicated. In the preventive model, the final number of animals per group was as follows: NC (n = 8), MASH + vehicle (n = 8), MASH + *L.lactis* CKDB001 (n = 6), and MASH + *L.plantarum* Q180 (n = 8). For qPCR and immunoblot analyses, samples were pooled within each group and analyzed as independent pooled biological replicates. Data are presented as mean ± SD. Statistical significance was determined by one-way ANOVA with Tukey's multiple comparisons test: *P < 0.05, **P < 0.01, ***P < 0.001, ****P < 0.0001. (For interpretation of the references to color in this figure legend, the reader is referred to the Web version of this article.)

systemic metabolic function. Serum triglyceride (TG) levels were also not significantly elevated in the MASH groups despite evident hepatic pathology (Fig. S4D), further supporting the obesity-independent metabolic features of this model. These findings are consistent with previous reports that insulin resistance can be variable or less pronounced in lean MASH [7,28,29]. Together, these data suggest that this model exhibits lean-like, obesity-independent metabolic features of MASH, although it does not encompass the full clinical heterogeneity of human lean MASH. In contrast, mesenteric white adipose tissue (mWAT) weight was partially restored in the *L. lactis* CKDB001-treated group compared with the MASH vehicle group, whereas no significant change was observed in the *L. plantarum* Q180-treated group (Fig. 1C). Serum alanine aminotransferase (ALT), alkaline phosphatase (ALP), total cholesterol (TCHO), and TCHO/HDL-C ratio were increased in the MASH groups relative to the NC group, but were not significantly improved by probiotic treatment (Fig. S1D–E). In contrast, histological analysis of liver sections revealed that hepatocellular ballooning was attenuated in both microbe-treated groups, as assessed by hematoxylin and eosin (H&E) staining (Fig. 1D). Consistent with these results, Oil Red O (ORO) staining demonstrated a reduction in hepatic lipid accumulation following probiotic administration, with statistically significant attenuation observed in the *L. plantarum* Q180-treated group compared with the MASH vehicle group (Fig. 1D and E). In line with these findings, hepatic triglyceride (TG) content was reduced in the *L. plantarum* Q180-treated group relative to the MASH vehicle group, showing a pattern consistent with the ORO staining results (Fig. 1F). Consistent with the improvements in hepatic steatosis, hepatic expression of the inflammatory cytokines TNFα (Fig. 1J) and IL-6 (Fig. 1K), as assessed by ELISA in liver tissue homogenates, were reduced in both probiotic treatment groups compared with the MASH vehicle group. Immunoblot analysis of liver homogenates further demonstrated clear attenuation of inflammatory signaling in mice treated with either *L. lactis* CKDB001 or *L. plantarum* Q180 relative to the MASH vehicle group (Fig. S1F). In contrast, hepatic mRNA expression of macrophage and inflammatory markers, including *Adgre1*, *Il-1β*, *Ccl2*, and *Tnfα*, as determined by quantitative PCR, was robustly upregulated in the MASH groups compared with the NC group. Microbial treatment did not result in statistically significant attenuation of hepatic mRNA expression of these markers; however, the mice treated with *L. plantarum* Q180 exhibited a consistent trend toward reduced expression compared with the MASH vehicle group (Fig. S1H). Collectively, these results indicate that probiotic treatment effectively alleviates hepatic steatosis and inflammation in a MASH preventive model, while exerting modest modulatory effects on inflammatory gene expression.

3.2. Probiotic treatment attenuates hepatic fibrosis in a MASH preventive model

To assess the effects of probiotic administration on hepatic fibrogenesis, we subjected liver sections to Masson's trichrome and Sirius Red staining. Both histological analyses revealed a marked increase in fibrotic deposition in MASH mice compared with NC mice, which was attenuated by treatment with either *L. lactis* CKDB001 or *L. plantarum* Q180, as evidenced by reduced collagen deposition in liver tissue (Fig. 1D, G, and H). Consistent with the histological findings, immunoblot analysis of liver tissue demonstrated that the expression levels of collagen type I alpha 1 (COL1A1) and α-smooth muscle actin (αSMA) were significantly reduced in both microbe-treated groups compared with the MASH vehicle group (Fig. 1I). Quantitative PCR analysis further supported these observations, revealing a trend toward decreased expression of fibrogenic genes (*Acta2*, *Tgfβ*, *Col1a1*, *Col3a1*) in mice treated with either *L. lactis* CKDB001 or *L. plantarum* Q180, although the magnitude of reduction was less pronounced than that observed at the protein level (Fig. 1L). In addition, hepatic hydroxyproline content, a biochemical indicator of collagen accumulation, was significantly reduced in the *L. plantarum* Q180-treated group compared with the MASH vehicle group (Fig. S1G). Taken together, these results indicate that probiotic treatment effectively attenuates hepatic fibrotic remodeling in a MASH preventive model.

3.3. Probiotic treatment improves gut microbial composition and intestinal homeostasis in a MASH preventive model

To assess whether probiotic administration modulates the gut environment in a MASH preventive model, we analyzed fecal microbiota composition by 16S rRNA gene sequencing. Stacked bar plots demonstrated that MASH diet feeding markedly disrupted gut microbial community structure compared with that in the NC group, whereas administration of *L. lactis* CKDB001 or *L. plantarum* Q180 partially restored the relative abundance of dominant bacterial taxa toward a normal-like profile (Fig. 2A and B). Although administration of either probiotic strain did not significantly alter alpha diversity as assessed by the Chao1 index (Fig. 2C), beta diversity analysis visualized by principal coordinate analysis based on Bray–Curtis dissimilarity revealed a clear separation between the NC and MASH groups, as well as a distinct separation of probiotic-treated mice from MASH vehicle group along the PC2 axis, further supporting probiotic-induced remodeling of the gut microbial community (Fig. 2D).

To characterize taxonomic and functional alterations, we performed LEfSe and PICRUSt2 analyses. *Escherichia fergusonii*, *Prevotellamassilia timonensis*, *Bacteroides caecimuris*, and *Lactobacillus delbrueckii* were significantly enriched following *L. lactis* CKDB001 treatment, whereas *Faecalibaculum rodentium*, *Mucispirillum schaedleri*, *Ruthenibacterium lactatiformans*, *Enterobacter cloacae*, *Lactiplantibacillus plantarum*, and *Eubacterium coprostanoligenes* were significantly increased following *L. plantarum* Q180 treatment (Fig. 2E). The predicted abundance of the GSH metabolism pathway, inferred using PICRUSt2, showed a tendency to increase in the *L. lactis* CKDB001-treated group compared with the MASH vehicle group (Fig. 2F). To determine whether these predicted functional changes were reflected at the metabolite level, we measured GSH levels in the cecal contents. Probiotic treatment increased total glutathione levels compared with the MASH vehicle group (Fig. 2G). In addition, the GSH/GSSG ratio, an indicator of redox balance, was also elevated in probiotic-treated mice, indicating improved intestinal redox status (Fig. 2H). These findings suggest that probiotic-induced alterations in gut microbiota are associated with increased intestinal glutathione levels and improved redox homeostasis. Correlation analysis further demonstrated that the relative abundance of each administered probiotic strain was positively associated with the predicted abundance of the GSH metabolism pathway (Fig. 2I and J). To further validate these functional predictions at the genomic level, we performed whole genome sequencing (WGS) of the two probiotic strains (Table S1). Genomic analysis revealed that *L. plantarum* Q180 possesses a robust genetic repertoire for GSH biosynthesis, including the bifunctional gshF/AB and gshA genes, along with glutathione peroxidase (gpx). Additionally, *L. plantarum* Q180 harbors the glutamate transporter (yjeM) and glutamate dehydrogenase (gdhA), further supporting its metabolic capacity for GSH-related pathways. In contrast, while *L. lactis* CKDB001 lacks the de novo GSH biosynthetic genes, it carries the glutamate ABC transporter (glub) and cysteine synthase (cysK), suggesting a specialized role in providing essential amino acid precursors. Both strains had core redox control genes, specifically thioredoxin (trxA) and thioredoxin-disulfide reductase (trxB), as well as cysteine synthase family proteins (cysK-like and metB/cysK). Collectively, these genomic features provide supportive genomic evidence for the potential involvement of the administered strains in GSH-related metabolic processes. Given the close association between microbial-derived redox factors and epithelial barrier function, we next examined intestinal tight junction integrity. Immunoblotting and quantitative analysis revealed that the protein expression of the tight junction marker occludin, which was markedly reduced in MASH vehicle group compared with NC group, was effectively restored by probiotic treatment (Fig. S3A).

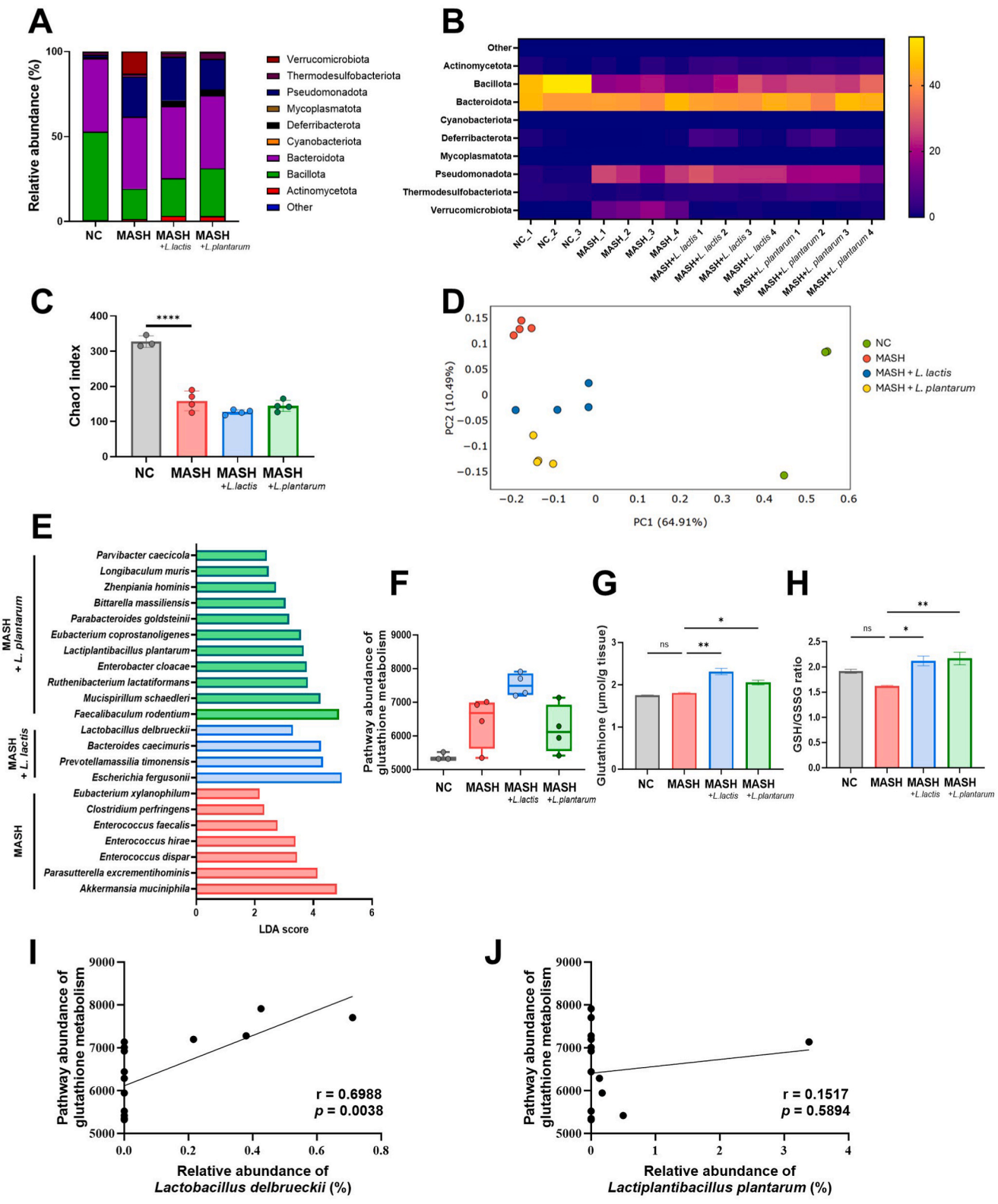

Fig. 2. Preventive Administration of *L. lactis* CKDB001 and *L. plantarum* Q180 Improves Gut Environment and Microbial Balance.
Relative abundance of fecal microbiota at the phylum level shown as stacked bar plots for each experimental group (A) and each sample (B). Alpha diversity assessed by the Chao1 index (C). Beta diversity analysis visualized by principal coordinate analysis (PCoA) based on Bray–Curtis (D). Differentially abundant bacterial species identified by linear discriminant analysis effect size (LEfSe) following administration of *L. lactis* CKDB001 or *L. plantarum* Q180 (E). Predicted abundance of the glutathione metabolism pathway inferred using PICRUSt2 (F). Glutathione levels measured in cecal contents (G) and GSH/GSSG ratio as an indicator of intestinal redox balance (H). Correlation analysis between the relative abundance of treated probiotic species and the predicted abundance of the glutathione metabolism pathway (I, J). Sample size and replicate definitions are as described in Fig. 1. Data are presented as mean ± SD. Statistical significance was determined as described in the Methods.

Immunohistochemical staining further confirmed improved localization and continuity of tight junction protein along the intestinal epithelium in the probiotic-treated mice (Fig. S3B and C). Histological examination by H&E staining showed that probiotic administration also alleviated MASH diet-induced epithelial damage (Fig. S3B). Taken together, these results indicate that probiotic treatment reshapes gut microbial composition and preserves intestinal barrier integrity, thereby restoring intestinal homeostasis in a MASH preventive model.

3.4. Probiotic treatment attenuates hepatic oxidative stress and enhances antioxidant responses in a MASH preventive model

Given that probiotic administration reshaped gut microbial composition and enriched bacterial taxa positively associated with intestinal GSH levels, we next asked whether these gut redox alterations translated into reduced hepatic oxidative stress in MASH. Hepatic ROS levels were first evaluated by dihydroethidium staining, which showed markedly increased fluorescence in the MASH vehicle group but a significant reduction in both microbe-treated groups (Fig. 3A and B). Consistently, TUNEL assays demonstrated that probiotic treatment attenuated oxidative stress-associated hepatocellular injury, as evidenced by a decreased percentage of TUNEL-positive cells compared with the MASH vehicle group (Fig. 3C and D). We further assessed oxidative damage by immunohistochemistry for 3-nitrotyrosine (3-NT) and 4-hydroxynonenal (4-HNE), markers of protein nitration and lipid peroxidation, respectively. Both markers were elevated in MASH vehicle livers but were reduced following probiotic treatment, with decreased positive staining areas (Fig. 3E–G). Finally, to determine whether these antioxidant effects were linked to activation of hepatic Nrf2 signaling, we assessed Nrf2 protein levels and target gene expression. Hepatic Nrf2 expression was increased in probiotic-treated groups compared with MASH vehicle group (Fig. 3E and H). Consistently, immunoblot analysis demonstrated increased nuclear accumulation of Nrf2 along with elevated expression of its downstream targets, HO-1 and NQO1 (Fig. 3I, Fig. S6A–C). Furthermore, quantitative PCR analysis revealed significant upregulation of Gsta1, Ho-1, and Nqo1 in probiotic-treated livers relative to the MASH vehicle group (Fig. 3J), supporting activation of the Nrf2-dependent antioxidant program in response to the probiotics. In parallel, probiotic treatment restored hepatic GSH levels and improved hepatic GSH/GSSG balance compared with the MASH vehicle group (Fig. S7A–B), further supporting enhanced hepatic redox homeostasis in the preventive model. These findings suggest that probiotic treatment alleviates hepatic oxidative stress in association with enhanced hepatic Nrf2 signaling and antioxidant responses in a MASH preventive model.

3.5. Probiotic treatment reduces hepatic steatosis and inflammation in a MASH therapeutic model

To evaluate the therapeutic effects of *L. lactis* CKDB001 and *L. plantarum* Q180 after MASH establishment, we fed mice NC or a MASH diet for 4 weeks to induce disease and then continued the same diet with concurrent administration of PBS (vehicle) or the microbial strains at different doses for an additional 4 weeks (Fig. 4A). During the treatment phase, mice received oral administration of the respective strains five times per week. To characterize the disease status at treatment initiation, hepatic fibrosis was assessed at 4 and 8 weeks of MASH diet feeding. Histological and molecular analyses demonstrated that MASH-associated fibrotic changes were already established at 4 weeks and further progressed by 8 weeks, as evidenced by increased collagen deposition and upregulation of fibrogenic markers (Fig. S5). These findings indicate that probiotic treatment was initiated after MASH establishment and continued during ongoing disease progression. Liver weight and liver-to-body weight ratio were significantly increased in all MASH groups compared with NC group (Fig. 4B). Body weight was monitored weekly, and gross examination of liver morphology at sacrifice revealed no overt macroscopic differences among the MASH groups (Fig. S2A–B). Consistent with findings from the MASH preventive model, the weights of eWAT and sWAT were reduced in the MASH group compared with the NC group, with no apparent differences attributable to microbial treatment (Fig. S2C). In contrast, mWAT weight exhibited a modest tendency toward restoration in probiotic-treated mice compared with MASH vehicle group, although this difference did not reach statistical significance (Fig. S2C). Histological analysis of liver sections by H&E staining demonstrated a reduction in hepatocellular ballooning in the probiotic-treated groups (Fig. 4D). ORO staining further revealed decreased hepatic lipid accumulation following probiotic administration (Fig. 4D and F); however, hepatic triglyceride (TG) content showed a decreasing trend only in the *L. plantarum* Q180-treated group compared with the MASH vehicle group (Fig. S2G). Similarly, serum alanine aminotransferase (ALT) and aspartate aminotransferase (AST) levels were elevated in MASH mice compared with NC group. Probiotic treatment did not result in statistically significant reductions in transaminase levels; however, both *L. lactis* CKDB001-fed mice and *L. plantarum* Q180-fed mice exhibited a consistent trend toward lower ALT and AST levels relative to the MASH vehicle group (Fig. S2D). Likewise, serum total cholesterol levels and the total cholesterol-to-HDL ratio were increased by the MASH diet, and although probiotic treatment did not significantly alter these parameters, mice treated with either bacterial strain showed a modest trend toward partial normalization compared with the MASH vehicle group (Fig. S2E). With respect to hepatic inflammation, immunoblot and quantitative PCR analyses did not reveal a clear reduction in inflammatory markers in either probiotic-treated group compared with the MASH vehicle group (Fig. S2F and I). Nevertheless, hepatic IL-6 levels were reduced in both probiotic-treated groups relative to the MASH vehicle group (Fig. 4E), whereas TNFα expression was significantly decreased only in the *L. plantarum* Q180-treated group (Fig. S2H). Together, these findings indicate that probiotic treatment partially alleviates hepatic steatosis and selectively modulates inflammatory responses in a MASH therapeutic model, with *L. plantarum* Q180 showing more pronounced effects on lipid accumulation and pro-inflammatory cytokine expression.

3.6. Probiotic treatment attenuates hepatic fibrosis in a MASH therapeutic model

Therapeutic administration of *L. lactis* CKDB001 or *L. plantarum* Q180 significantly attenuated hepatic fibrosis in the MASH therapeutic model. Masson's trichrome and Sirius Red staining of liver sections revealed a marked reduction of collagen deposition in both probiotic-treated groups (Fig. 4D, G, and 4H). Consistent with these histological findings, immunoblot analysis of liver tissue demonstrated decreased expression of the fibrotic markers fibronectin (FN) and αSMA (Fig. 4I). Notably, quantitative PCR analysis showed that mRNA expression levels of multiple fibrogenic genes, including *Acta2*, *Tgfβ*, *Col1a1*, and *Col3a1*, were significantly reduced in the probiotic-treated groups (Fig. 4J). These results demonstrate that probiotic treatment consistently attenuates hepatic fibrotic remodeling in a MASH therapeutic model.

3.7. Probiotic treatment improves gut microbial composition and intestinal homeostasis in a MASH therapeutic model

To assess the therapeutic and dose-dependent effects of each probiotic strain on MASH, we analyzed fecal microbiota composition by 16S rRNA gene sequencing. Stacked bar plots demonstrated that MASH diet feeding markedly disrupted gut microbial community structure compared with that in the NC group, and administration of either low or high doses of *L. lactis* CKDB001 or *L. plantarum* Q180 did not restore the relative abundance of dominant bacterial taxa toward a normal-like profile (Fig. 5A and B). Consistent with these results, administration of either probiotic strain did not significantly alter alpha or beta diversity compared with that in the MASH vehicle group (Fig. 5C and D). To

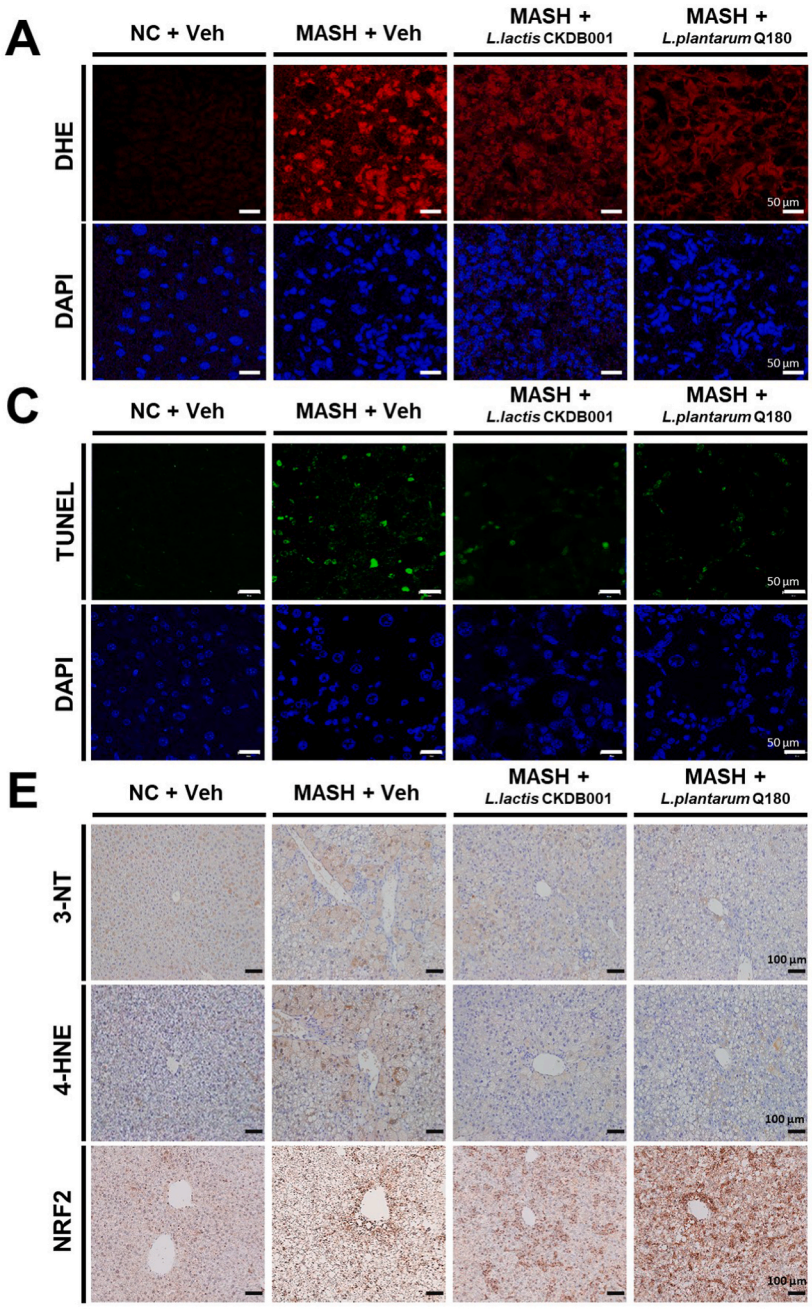

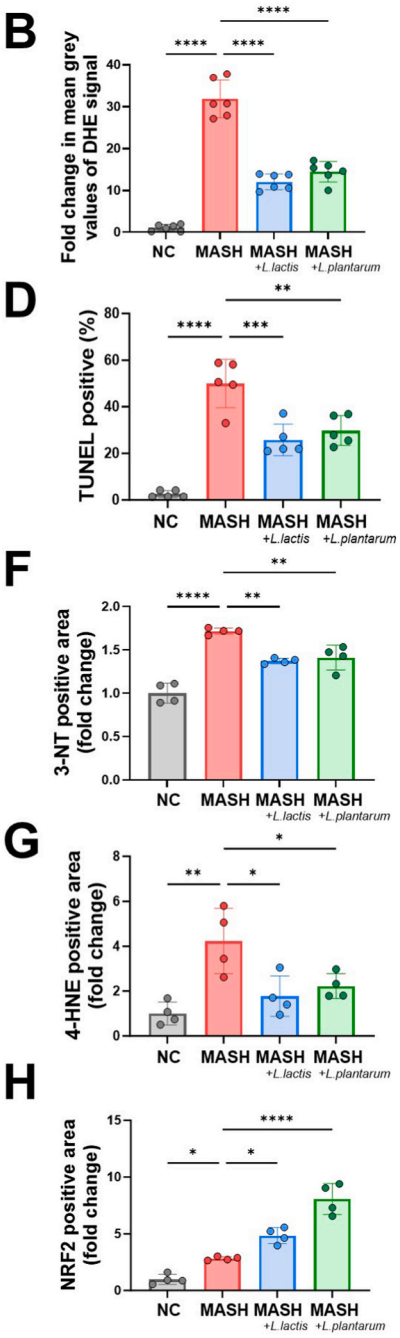

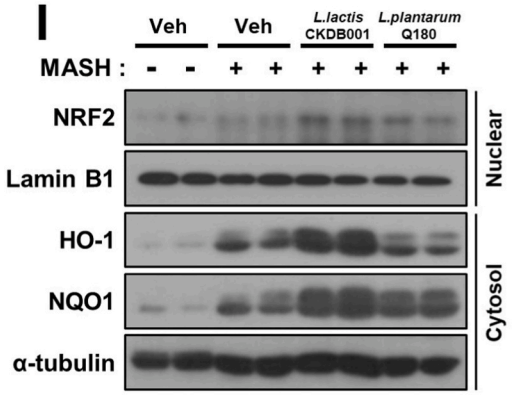

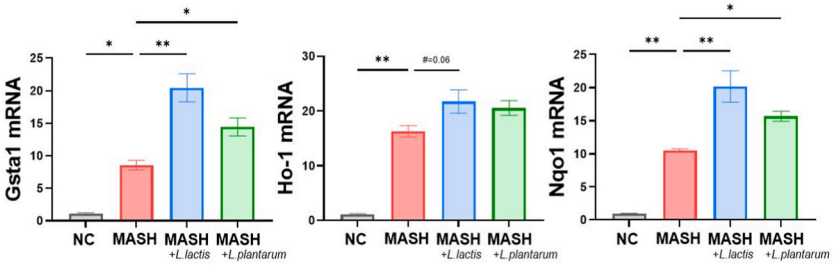

(caption on next page)

Fig. 3. Enhanced Hepatic Nrf2-Associated Antioxidant Responses and Reduced Oxidative Stress Underlie the Anti-MASH Effects of *L. lactis* CKDB001 and *L. plantarum* Q180.

Representative liver cryosections (5 μm) stained with DHE and counterstained with DAPI (A). Quantification of DHE fluorescence as fold change in mean gray value (B). Representative liver sections (paraffin-embedded) stained for TUNEL assay and counterstained with DAPI (C). Quantification of TUNEL-positive cells, expressed as a percentage (%) (D). Representative liver sections immunostained for 3-nitrotyrosine (3-NT), 4-hydroxynonenal (4-HNE), and NRF2. Scale bars, 100 μm (E). Quantification of 3-NT, 4-HNE, and NRF2-positive areas, expressed as fold change (F-H). Immunoblot analysis of nuclear and cytosolic fractions from liver tissues showing protein levels of NRF2 (nuclear fraction), and its downstream targets HO-1 and NQO1 (cytosolic fraction) in the indicated groups. Lamin B1 (nuclear marker) and α-tubulin (cytosolic marker) were used as loading controls (I). Hepatic mRNA levels of Nrf2 target genes, *Gsta1, Ho-1,* and *Nqo1* (J). Sample size and replicate definitions are as described in Fig. 1. Data are presented as mean ± SD. Statistical significance was determined by one-way ANOVA with Tukey's multiple comparisons test: *P < 0.05, **P < 0.01, ***P < 0.001, ****P < 0.0001.

characterize taxonomic and functional alterations, LEfSe and PICRUSt2 analyses were performed. *Akkermansia muciniphila*, *Parasutterella excrementihominis*, and *Mediterraneibacter butyricigenes* were significantly enriched following low-dose *L. lactis* CKDB001 administration, whereas *Faecalibaculum rodentium*, *Lactobacillus delbrueckii*, and *Parabacteroides goldsteinii* were significantly increased following high-dose *L. lactis* CKDB001 treatment. *Lactiplantibacillus plantarum* was significantly enriched in the high-dose *L. plantarum* Q180-treated group (Fig. 5E). The predicted abundance of the microbial GSH metabolism pathway, inferred using PICRUSt2, did not increase in any probiotic-treated group compared with that in the MASH vehicle group (Fig. 5F). To determine whether these predicted functional changes were reflected at the metabolite level, we measured glutathione levels in the cecal contents. Notably, despite the lack of a significant increase in the predicted pathway abundance, probiotic treatment increased total glutathione levels compared with the MASH vehicle group (Fig. 5G). Furthermore, the GSH/GSSG ratio was elevated in probiotic-treated mice, indicating improved intestinal redox balance (Fig. 5H). Correlation analysis further demonstrated that the relative abundance of each administered probiotic species was positively associated with the predicted abundance of the microbial GSH metabolism pathway (Fig. 5I and J). These findings were further supported by WGS data, which confirmed the presence of functional redox-related genes in the administered strains (Table S1). Specifically, *L. plantarum* Q180 harbors a comprehensive GSH metabolic suite, including the bifunctional *gshF/AB*, *gshA*, and *gpx*, while *L. lactis* CKDB001 carries the glutamate ABC transporter *gluB* and cysteine synthase *cysK*. This strain-specific genetic repertoire may support potential involvement in GSH-related metabolic processes, despite limited global restructuring of the microbiome.

Given the close relationship between microbial-driven redox homeostasis and epithelial barrier integrity, we also examined intestinal tight junction structure. Immunoblotting and immunohistochemical analyses revealed that the expression and epithelial localization of occludin were significantly reduced in MASH mice but partially restored following probiotic treatment (Figs. S3D, S3E, and S3F). Histological examination further showed attenuation of MASH-induced epithelial damage in the probiotic-treated animals (Fig. S3E). Consistent with improved barrier integrity, circulating lipopolysaccharide (LPS) levels were significantly elevated in MASH mice and reduced following probiotic treatment, indicating decreased gut-to-liver translocation of endotoxin (Fig. 4C). Fecal LPS levels were also assessed, supporting the gut as a primary source of endotoxin (Fig. S2J). Overall, these findings indicate that therapeutic probiotic administration is associated with fecal detection of administered strains and preservation of GSH-associated microbial signatures, while exerting only limited effects on global gut microbiota composition in the presence of established MASH.

3.8. Probiotic treatment is associated with enhanced hepatic Nrf2 signaling and reduced oxidative stress in a MASH therapeutic model

Given that therapeutic probiotic administration preserved GSH-associated microbial signatures despite limited global changes in microbiota composition, we next asked whether these intestinal effects translated into reduced hepatic oxidative stress and enhanced antioxidant responses in the MASH therapeutic model. DHE staining revealed that hepatic ROS levels were markedly elevated in the MASH vehicle group but were significantly reduced following therapeutic administration of *L. lactis* CKDB001 or *L. plantarum* Q180 (Fig. 6A and B). Consistent with these results, the TUNEL assay demonstrated a decrease in hepatocellular death in both probiotic-treated groups compared with the MASH vehicle group, indicating attenuation of oxidative stress-associated liver injury (Fig. 6C and D). Immunohistochemical analyses further supported reduced oxidative damage, as staining for 3-NT and 4HNE was diminished in probiotic-treated livers relative to that in the MASH vehicle group (Fig. 6E–G). Finally, to determine whether these protective effects were associated with alterations in hepatic Nrf2 antioxidant signaling, we assessed Nrf2 protein levels and target gene expression. Hepatic NRF2 expression was increased in probiotic-treated groups compared with MASH vehicle group (Fig. 6E and H). Immunoblot analysis further confirmed increased nuclear accumulation of NRF2 along with elevated expression of its downstream targets, HO-1 and NQO1 (Fig. 6I and Fig. S6D–F). In parallel, quantitative PCR analysis showed significant upregulation of Nrf2-associated antioxidant genes, including *Gsta1*, *Ho-1*, and *Nqo1* in both probiotic-treated groups relative to the MASH vehicle group (Fig. 6J). In addition, hepatic GSH levels and hepatic GSH/GSSG ratio were significantly restored following probiotic treatment compared with the MASH vehicle group (Fig. S7C–D), indicating improved hepatic redox balance in the therapeutic model. Together, these findings indicate that probiotic administration enhances hepatic antioxidant responses and limits oxidative stress-associated liver injury in a MASH therapeutic model.

4. Discussion

MASH is a multifactorial liver disease in which oxidative stress and inflammatory signaling drive hepatocellular injury and fibrogenesis [30]. Importantly, an increasing proportion of patients has been found to develop MASH in the absence of obesity (i.e., lean MASH), highlighting obesity-independent mechanisms that sustain redox imbalance and liver damage [7,8]. Here, we show that oral administration of *L. lactis* CKDB001 or *L. plantarum* Q180 alleviates MASH pathology in association with a probiotic-associated gut–liver redox interaction. Across preventive and therapeutic settings, probiotic treatment improved steatosis and, more robustly, attenuated fibrotic remodeling, which was accompanied by modulation of microbial GSH-related capacity, enhanced hepatic Nrf2-associated antioxidant responses, and reduced oxidative stress markers.

Microbiome-targeted approaches have emerged as viable strategies to modulate diet-induced liver injury, including microbiome replacement to ameliorate steatohepatitis [31,32]. Our data extend this concept by suggesting that defined probiotic strains modulate a gut–liver redox interaction associated with intestinal glutathione levels, hepatic Nrf2 accumulation, and enhanced antioxidant gene expression. A central finding of this work is that increased intestinal glutathione levels were accompanied by increased hepatic nuclear Nrf2 accumulation and Nrf2-related antioxidant gene expression. Consistently, increased GSH levels were also observed in cecal contents, supporting enhanced intestinal redox capacity at the site of microbial activity. In parallel, probiotic treatment restored hepatic GSH levels and improved hepatic GSH/GSSG balance, supporting enhanced hepatic redox homeostasis in

association with the observed intestinal redox changes. WGS revealed that *L. plantarum* Q180 harbors genes associated with GSH biosynthesis (e.g., gshF/AB, gshA, and gpx), indicating the potential for de novo GSH production [33]. In contrast, *L. lactis* CKDB001 lacks canonical GSH biosynthetic genes but encodes glutamate transport (gluB) and cysteine synthesis (cysK), suggesting a complementary role in supporting GSH metabolism via precursor availability [34]. Furthermore, the presence of the thioredoxin system [35] (trxA and trxB) in both strains, alongside

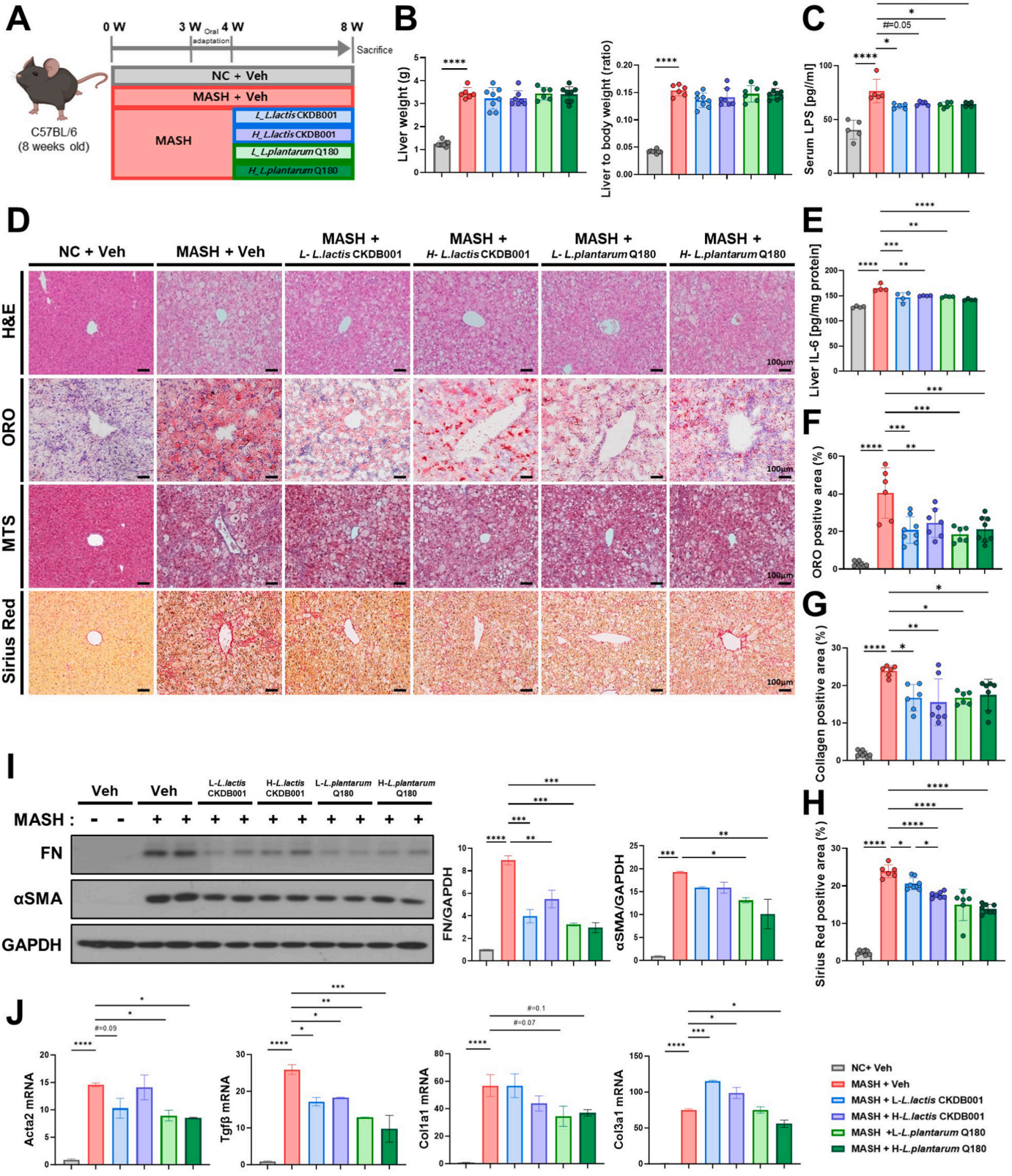

(caption on next page)

Fig. 4. Therapeutic Effects of *L. lactis* CKDB001 and *L. plantarum* Q180 in Reducing Hepatic Lipid Accumulation, Inflammation, and Fibrosis in a MASH Model.

Experimental scheme: 8-week-old C57BL/6 mice were acclimated for 1 week and then fed either a normal chow diet (NC) or a high-fat, high-cholesterol, high-fructose (HFHCF) diet (MASH) for 4 weeks, followed by oral gavage of bacterial strains for an additional 4 weeks while maintaining the respective diets at either a low dose (L; 1.0×10^9 CFU/day) or a high dose (H; 5.0×10^9 CFU/day) (A). Liver weight (g) and liver-to-body weight (B.W.) ratio (B), serum lipopolysaccharide (LPS) levels (C), representative liver sections stained with H&E, Oil Red O, Masson's trichrome (MTS), and Sirius Red, scale bars 100 μm (D). Liver IL-6 levels (E), quantification of Oil Red positive area (%) (F), quantification of collagen area (%) and Sirius red collagen area (%) (G, H). Immunoblot analysis of FN (Fibronectin) and αSMA in liver lysates with GAPDH as a loading control and quantification of protein levels (I), and hepatic mRNA levels of *Acta2*, *Tgfβ, Col1a1,* and *Col3a1* (J). Each data point represents an individual mouse (biological replicate), unless otherwise indicated. In the therapeutic model, The final number of animals per group was as follows: NC + Veh (n = 8), MASH + Veh (n = 6), MASH + L-*L.lactis* CKDB001 (n = 8), MASH + H-*L.lactis* CKDB001 (n = 7), MASH + L-*L.plantarum* Q180 (n = 6), and MASH + H-*L.plantarum* Q180 (n = 8). For qPCR and immunoblot analyses, samples were pooled within each group and analyzed as independent pooled biological replicates. Data are presented as mean ± SD. Statistical significance was determined by one-way ANOVA with Tukey's multiple comparisons test: *P < 0.05, **P < 0.01, ***P < 0.001, ****P < 0.0001. (For interpretation of the references to color in this figure legend, the reader is referred to the Web version of this article.)

their respective glutamate transport systems (yjeM for *L. plantarum* Q180 and gluB for *L. lactis* CKDB001), suggests the potential to support redox balance within the gut lumen. Together, these findings support a model in which distinct probiotic strains may contribute to the microbial GSH pool through different but potentially complementary mechanisms.

Nrf2 is a master transcriptional regulator of detoxification and antioxidant genes, and impaired Nrf2 signaling has been implicated in MASH-associated oxidative injury [36,37]. Probiotic treatment increased hepatic expression of canonical Nrf2 targets and reduced multiple indices of oxidative damage, including superoxide-associated signals, protein nitration, and lipid peroxidation. While our data support an association with enhanced hepatic Nrf2 signaling, we did not directly test the requirement of Nrf2 using loss-of-function approaches. Future studies employing genetic or pharmacological inhibition of Nrf2 will be necessary to establish causality. Nevertheless, our previous studies using genetic and pharmacological approaches have established a causal protective role of Nrf2 in steatohepatitis [26,38]. In the MASH therapeutic model, reduced hepatocellular death following probiotic treatment may further support functional restoration of hepatic redox resilience.

Our results underscore the intestine as an upstream determinant of hepatic redox homeostasis. Improved intestinal barrier integrity may reduce portal delivery of gut-derived pro-inflammatory and pro-oxidant cues, thereby lowering hepatic oxidative burden. Consistent with this, improved barrier integrity was associated with reduced circulating endotoxin levels, supporting a functional link between gut barrier restoration and hepatic redox modulation. Further studies will be required to define the precise causal mechanisms underlying this axis. In the preventive model, probiotics improved microbial richness and epithelial barrier integrity, and microbial taxa responsive to probiotic treatments correlated positively with intestinal GSH. In the therapeutic model, global microbiome shifts were limited, which is consistent with reduced community plasticity in the presence of established disease and the shorter intervention window compared with the preventive model; nevertheless, functional redox-associated signatures were maintained alongside reduced hepatic oxidative stress. This suggests that therapeutic benefit does not strictly require wholesale microbiome remodeling but depends on the targeted strain-associated metabolic potential related to glutathione metabolism.

We next evaluated probiotic-induced alterations in gut microbiota using fecal samples from both preventive and therapeutic models. In both models, the administered strains, *L. lactis* CKDB001 and *L. plantarum* Q180, were detected in fecal samples, indicating intestinal exposure and detectable presence following administration. Probiotic treatment was associated with an increased abundance of bacterial species that have been reported to exert beneficial effects on host metabolic and intestinal health. Notably, *A. muciniphila*, a mucin-degrading bacterium linked to enhanced gut barrier integrity, reduced inflammation, and improved metabolic homeostasis [39], was enriched in the probiotic-treated groups. Similarly, *P. goldsteinii*, which has been associated with anti-inflammatory effects and protection against diet-induced metabolic dysfunction [40], and *M. butyricigenes*, a putative butyrate-producing bacterium implicated in intestinal epithelial health and immune regulation [41], were increased following probiotic administration. In parallel, PICRUSt2-based functional prediction suggested a modest increase in GSH metabolism pathway, and correlation analysis revealed positive association between the administered strains and predicted redox-related functions. Although these findings are based on inferred profiles, they are consistent with an association between probiotic-driven microbiome modulation and altered intestinal redox status.

The robust anti-fibrotic phenotype in the probiotic-treated mice may reflect the sensitivity of fibrogenic remodeling to redox imbalance. ROS not only amplify inflammatory cues but also promote hepatic stellate cell activation and extracellular matrix remodeling, including collagen deposition and stabilization. Thus, Nrf2-driven antioxidant reinforcement may interrupt these redox-dependent, pro-fibrotic circuits, leading to disproportionately larger effects on fibrosis than on steatosis. This concept is consistent with our observation that multiple oxidative damage indices were reduced across both preventive and therapeutic models. Although our data consistently show increased microbial glutathione levels, enhanced hepatic Nrf2-associated antioxidant responses, and reduced oxidative stress, the current study does not establish a direct causal role of glutathione in mediating these effects. Pharmacological inhibition of glutathione synthesis (e.g., using buthionine sulfoximine, BSO) would provide additional insight into the causal contribution of glutathione and should be explored in future studies.

Anti-fibrotic efficacy was consistently observed in both preventive and therapeutic models, supported by reduced collagen deposition and decreased fibrosis-associated markers. Because the fibrosis stage is a major determinant of clinical outcomes [42], this dual validation strengthens the translational relevance of our results. Although several inflammatory transcripts were not uniformly reduced at the endpoint, selective decreases in cytokines (e.g., IL-6 and TNFα) and robust improvements in redox injury support a model in which Nrf2-driven redox reinforcement precedes broader inflammatory resolution under ongoing dietary challenge. Notably, the effects on steatosis and metabolic parameters were more modest or variable, suggesting that the primary strength of probiotic intervention lies in fibrosis attenuation and redox-associated protection rather than complete reversal of all MASH features.

The relevance of our results to lean MASH is particularly notable. Our diet paradigm recapitulated features of a lean MASH-like phenotype [7], with fibrogenesis and oxidative injury developing despite reduced adiposity (as assessed by body weight and fat mass), indicating obesity-independent disease mechanisms. However, this model represents a defined experimental system rather than the full clinical spectrum of human lean MASH. Although it reproduces key features of lean MASH, the relatively severe dietary conditions may not fully capture the biological heterogeneity observed in patients. Nonetheless, redox-targeted strategies that operate independently of weight loss may

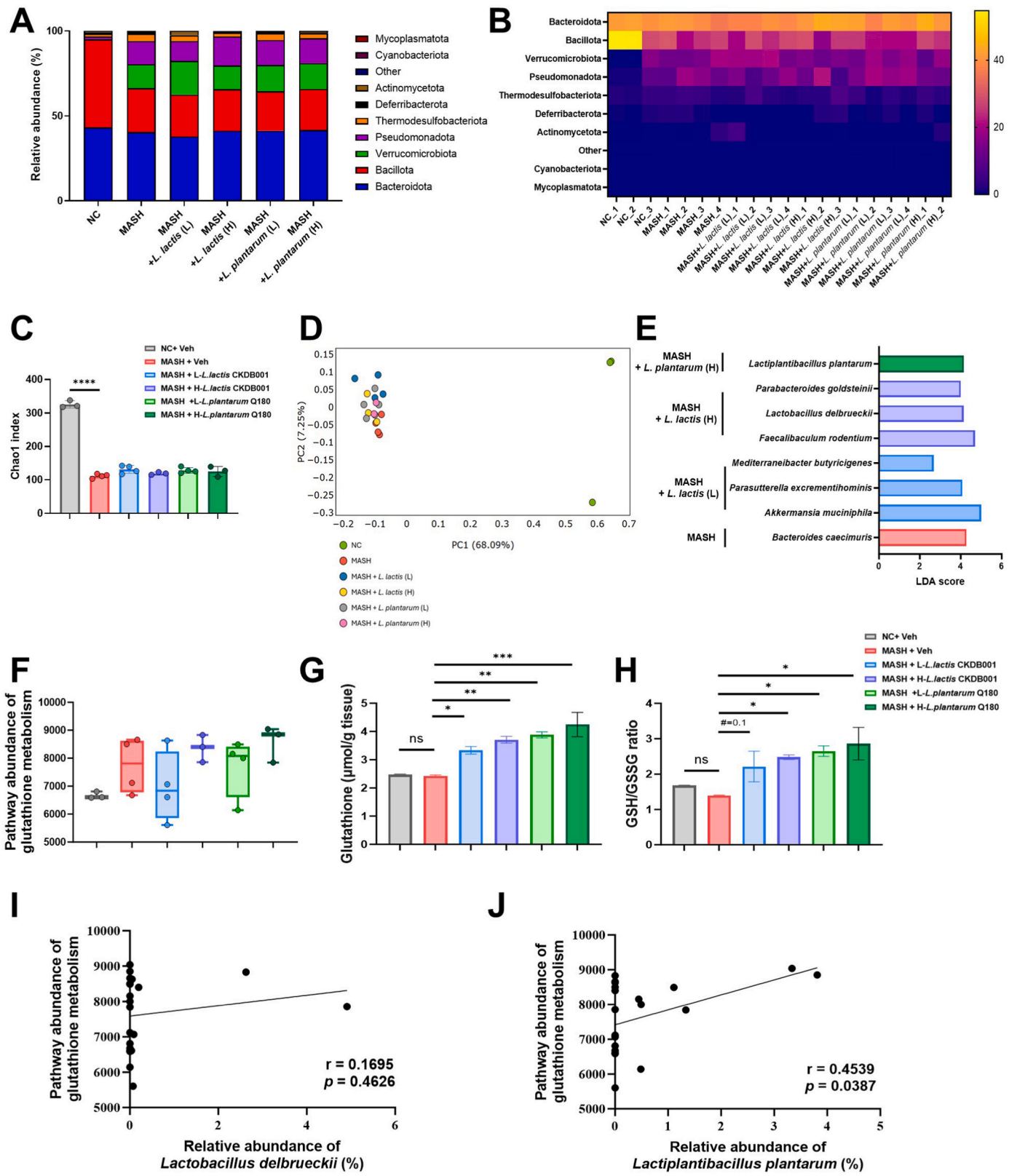

Fig. 5. Therapeutic Administration of *L. lactis* CKDB001 and *L. plantarum* Q180 Improves Gut Environment and Microbial Balance.
Relative abundance of fecal microbiota at the phylum level shown as stacked bar plots for each experimental group (A) and each sample (B). Alpha diversity assessed by the Chao1 index (C). Beta diversity analysis visualized by principal coordinate analysis (PCoA) based on Bray–Curtis (D). Differentially abundant bacterial species identified by linear discriminant analysis effect size (LEfSe) following administration of low or high of *L. lactis* CKDB001 or *L. plantarum* Q180 (E). Predicted abundance of the glutathione metabolism pathway inferred using PICRUSt2 (F). Glutathione levels measured in cecal contents (G) and GSH/GSSG ratio as an indicator of intestinal redox balance (H). Correlation analysis between the relative abundance of treated probiotic species and the predicted abundance of the glutathione metabolism pathway (I, J). Sample size and replicate definitions are as described in Fig. 4. Data are presented as mean ± SD. Statistical significance was determined as described in the Methods.

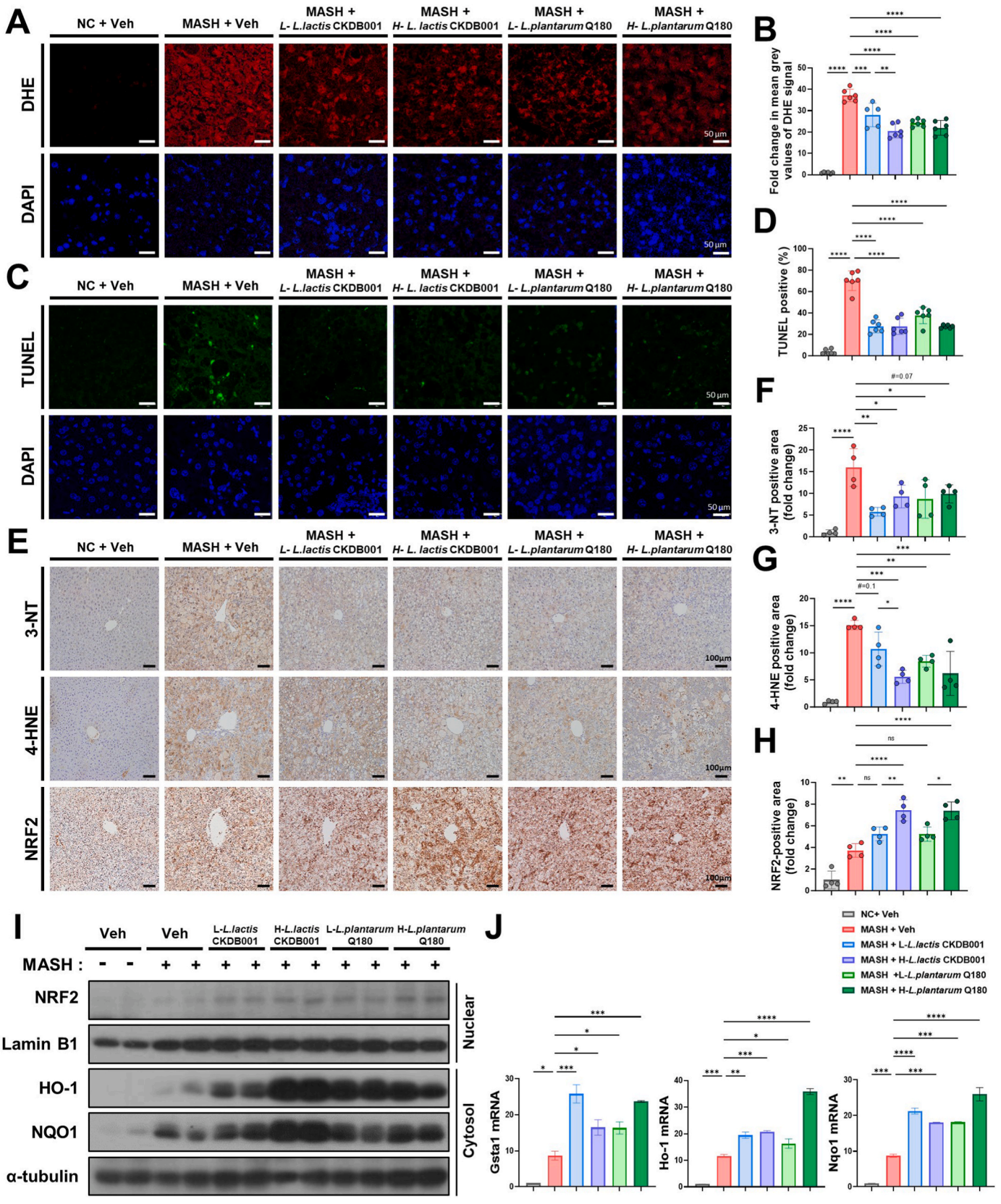

(caption on next page)

Fig. 6. *L. lactis* CKDB001 and *L. plantarum* Q180 Are Associated with Enhanced Hepatic Nrf2 Signaling and Reduced Oxidative Stress Following Therapeutic Administration.
Representative liver cryosections (5 μm) stained with DHE and counterstained with DAPI (A). Quantification of DHE fluorescence as fold change in mean gray value (B). Representative liver sections (paraffin-embedded) stained for TUNEL assay and counterstained with DAPI (C). Quantification of TUNEL-positive cells, expressed as a percentage (%) (D). Representative liver sections immunostained for 3-nitrotyrosine (3-NT), 4-hydroxynonenal (4-HNE), and NRF2. Scale bars, 100 μm (E). Quantification of 3-NT, 4-HNE, and NRF2–positive areas, expressed as fold change (F-H). Immunoblot analysis of nuclear and cytosolic fractions from liver tissues showing protein levels of NRF2 (nuclear fraction), and its downstream targets HO-1 and NQO1 (cytosolic fraction) in the indicated groups. Lamin B1 (nuclear marker) and α-tubulin (cytosolic marker) were used as loading controls (I). Hepatic mRNA levels of Nrf2 target genes, *Gsta1, Ho-1, and Nqo1* (J). Sample size and replicate definitions are as described in Fig. 4. Data are presented as mean ± SD. Statistical significance was determined by one-way ANOVA with Tukey's multiple comparisons test: *P < 0.05, **P < 0.01, ***P < 0.001, ****P < 0.0001, ns = not significant.

address an unmet need in lean MASH populations.

Several limitations warrant consideration. While our WGS data provide a genetic rationale for microbial GSH metabolism, the current study did not directly assess in vivo expression or enzymatic activity of GSH-related genes, nor did it quantify intermediate metabolites of the γ-glutamyl cycle, including γ-glutamylcysteine, cysteine, S-lactoylglutathione, and 5-oxoproline. Therefore, the proposed contribution of microbial GSH metabolism should be interpreted as functional potential rather than definitive metabolic activity. In addition, transcriptomic or proteomic validation of microbial GSH-related pathways was not performed in the current study. Although we incorporated GSH-based redox measurements, including GSH and GSH/GSSG balance, additional metabolomic and enzyme-level analyses will be important to further define mechanistic redox flux between the intestine and liver. In addition, while PICRUSt2 provided predictive functional insights, and 16S rRNA sequencing supported treatment-associated microbial alterations, integrated metagenomic and metabolomics approaches will be required to more comprehensively define microbial contributions to gut–liver redox signaling. Longer therapeutic dosing and follow-up studies are also needed to evaluate durability and translational potential.

In summary, *L. lactis* CKDB001 and *L. plantarum* Q180 are associated with gut–liver redox crosstalk, accompanied by increased intestinal GSH levels and enhanced hepatic antioxidant responses associated with Nrf2 signaling. The reproducible protection observed in preventive and therapeutic models-particularly the consistent attenuation of fibrosis—supports the therapeutic promise of defined probiotic strategies to treat redox-driven MASH, including lean MASH.

5. Conclusions

This study supports the presence of a probiotic-associated gut–liver redox interaction linked to attenuation of MASH progression. Oral administration of *L. lactis* CKDB001 or *L. plantarum* Q180 was associated with altered intestinal glutathione redox status, activation of hepatic Nrf2 signaling, and reduction of oxidative stress-associated liver injury. These effects were accompanied by improved steatosis and marked attenuation of fibrosis in both preventive and therapeutic MASH models. Collectively, our findings support microbiome-based redox modulation as a mechanistically informed and promising therapeutic strategy for MASH.

Ethical statement

All animal experiments were approved by the Institutional Animal Care and Use Committee (IACUC) of Yonsei University College of Medicine (IACUC: 2023-0164) and were performed in accordance with the relevant guidelines and regulations.

Funding

This work was supported by National Research Foundation of Korea (NRF) grants funded by the Korea government (MSIT) (RS-2024-00354430 to H.W.L.; RS-2025-18362970; RS-2025-00514319; RS-2022-NR070091 to S.H.B.; RS-2026-25483580, RS-2021-NR062133 to D.H. L.); a Faculty Research Grant from the Yonsei University College of Medicine (6-2019-0068 to S.H. Bae); the POSCO Science Fellowship of POSCO TJ Park Foundation (D.H.L.); and the ABC-based Regenerative BioTherapeutics (ABC project) grant funded by the Korea government (MSIT, the Ministry of Health & Welfare) (RS-2024-00432653 to S.H. Bae). This study was also supported by research funding from Chong Kun Dang Bio Corp (4-2024-1426 to H.W.L.).

CRediT authorship contribution statement

Da Hyun Lee: Data curation, Investigation, Methodology, Project administration, Validation, Visualization, Writing – original draft. **Da Ye Kim:** Investigation, Methodology, Project administration, Writing – original draft. **Hyunchae Joung:** Data curation, Formal analysis, Project administration, Software, Validation, Writing – original draft. **Hyolim Kim:** Methodology, Validation. **Yujin Jeon:** Investigation, Methodology. **Sunghee Lee:** Software, Validation. **Chang Hun Shin:** Resources, Software, Validation. **Yu Seol Lee:** Data curation, Investigation. **Ji Yun Bang:** Investigation, Methodology. **Eo Jin Lee:** Formal analysis, Investigation. **Shin Young Cha:** Formal analysis, Investigation. **Soo Han Bae:** Conceptualization, Data curation, Supervision, Writing – review & editing. **Hye Won Lee:** Conceptualization, Data curation, Supervision, Validation, Writing – review & editing.

Declaration of competing interest

Some authors are affiliated with CKDBio, which holds intellectual property rights and commercial interests in the bacterial strains used in this study. Specifically, *Lactobacillus delbrueckii subsp. lactis* CKDB001 (KCTC14149BP, KR10-2128098) is patented by CKDBio, and *Lactiplantibacillus plantarum* Q180 (KACC91865P) was transferred from the Korea Food 425 Research Institute to CKDBio and is commercially available as a health functional food product. These affiliations and commercial interests had no role in the study design, data collection, interpretation, or decision to publish. No other conflicts of interest relevant to this article have been declared.

Acknowledgements

The authors thank the animal facility at Yonsei University College of Medicine for providing animal housing and experimental infrastructure. We also acknowledge the Department of Pathology, Yonsei University College of Medicine, for histological processing and immunohistochemical staining. The authors also thank BioScience Writers, LLC, for editing support.

Appendix A. Supplementary data

Supplementary data to this article can be found online at https://doi.org/10.1016/j.freeradbiomed.2026.05.338.

Abbreviations

16S rRNA 16S ribosomal RNA
4-HNE 4-hydroxynonenal
3-NT 3-nitrotyrosine

Adgre1 adhesion G protein–coupled receptor E1 (F4/80)
ALT alanine aminotransferase
AST aspartate aminotransferase
CCL2 C–C motif chemokine ligand 2
Chao1 Chao1 richness index
DHE dihydroethidium
DPBS dulbecco's phosphate-buffered saline
eWAT epididymal white adipose tissue
FN fibronectin
GSH glutathione
Gsta1/GSTA1 glutathione S-transferase alpha 1
GST glutathione S-transferase
H&E hematoxylin and eosin
HBSS Hank's balanced salt solution
HDL high-density lipoprotein
HO-1 heme oxygenase-1
IL-1β interleukin-1 beta
IL-6 interleukin-6
MASH Metabolic dysfunction-associated steatohepatitis
mWAT mesenteric white adipose tissue
MTS Masson's trichrome staining
NASH nonalcoholic steatohepatitis
NC normal chow diet
Nqo1/NQO1 NAD(P)H quinone oxidoreductase 1
NRF2/Nrf2 nuclear factor erythroid 2–related factor 2
OCLN Occludin
ORO Oil Red O
PC2 principal coordinate 2
PCoA principal coordinate analysis
PBS phosphate-buffered saline
qPCR quantitative polymerase chain reaction
ROS reactive oxygen species
sWAT subcutaneous white adipose tissue
TGFβ transforming growth factor beta
TG triglyceride
TNFα tumor necrosis factor alpha
TUNEL terminal deoxynucleotidyl transferase dUTP nick end labeling
α-SMA alpha-smooth muscle actin
α-diversity alpha diversity
β-diversity beta diversity

Data availability

The 16S rRNA sequencing data and associated metadata have been deposited in the NCBI Sequence Read Archive under accession number PRJNA1414780. Additionally, the whole-genome sequences and annotations for *L. lactis* CKDB001 and *L. plantarum* Q180 have been deposited in the NCBI GenBank database under accession numbers CP145818.1 (BioProject PRJNA1078986) and CP073753.1 (BioProject PRJNA725347), respectively. All data relevant to the study are included in the article and its supplementary figures and tables.

References

[1] P. Rada, A. Gonzalez-Rodriguez, C. Garcia-Monzon, A.M. Valverde, Understanding lipotoxicity in NAFLD pathogenesis: is CD36 a key driver? Cell Death Dis. 11 (9) (2020) 802.
[2] M. Arrese, D. Cabrera, A.M. Kalergis, A.E. Feldstein, Innate immunity and inflammation in NAFLD/NASH, Dig. Dis. Sci. 61 (5) (2016) 1294–1303.
[3] H. Malhi, G.J. Gores, Cellular and molecular mechanisms of liver injury, Gastroenterology 134 (6) (2008) 1641–1654.
[4] K. Begriche, J. Massart, M.A. Robin, F. Bonnet, B. Fromenty, Mitochondrial adaptations and dysfunctions in nonalcoholic fatty liver disease, Hepatology 58 (4) (2013) 1497–1507.
[5] F. Nassir, J.A. Ibdah, Role of mitochondria in nonalcoholic fatty liver disease, Int. J. Mol. Sci. 15 (5) (2014) 8713–8742.
[6] H. Tilg, P.D. Cani, E.A. Mayer, Gut microbiome and liver diseases, Gut 65 (12) (2016) 2035–2044.
[7] F. Chen, S. Esmaili, G.B. Rogers, E. Bugianesi, S. Petta, G. Marchesini, A. Bayoumi, M. Metwally, M.K. Azardaryany, S. Coulter, J.M. Choo, R. Younes, C. Rosso, C. Liddle, L.A. Adams, A. Craxi, J. George, M. Eslam, Lean NAFLD: a distinct entity shaped by differential metabolic adaptation, Hepatology 71 (4) (2020) 1213–1227.
[8] Q. Ye, B. Zou, Y.H. Yeo, J. Li, D.Q. Huang, Y. Wu, H. Yang, C. Liu, L.Y. Kam, X.X. E. Tan, N. Chien, S. Trinh, L. Henry, C.D. Stave, T. Hosaka, R.C. Cheung, M. H. Nguyen, Global prevalence, incidence, and outcomes of non-obese or lean non-alcoholic fatty liver disease: a systematic review and meta-analysis, Lancet Gastroenterol. Hepatol. 5 (8) (2020) 739–752.
[9] S. Sookoian, C.J. Pirola, Resmetirom for treatment of MASH, Cell 187 (12) (2024) 2897–2897 e1.
[10] S.A. Harrison, P. Bedossa, C.D. Guy, J.M. Schattenberg, R. Loomba, R. Taub, D. Labriola, S.E. Moussa, G.W. Neff, M.E. Rinella, Q.M. Anstee, M.F. Abdelmalek, Z. Younossi, S.J. Baum, S. Francque, M.R. Charlton, P.N. Newsome, N. Lanthier, I. Schiefke, A. Mangia, J.M. Pericas, R. Patil, A.J. Sanyal, M. Noureddin, M. B. Bansal, N. Alkhouri, L. Castera, M. Rudraraju, V. Ratziu, M.-N. Investigators, A phase 3, randomized, controlled trial of resmetirom in NASH with liver fibrosis, N. Engl. J. Med. 390 (6) (2024) 497–509.
[11] A. Albillos, A. de Gottardi, M. Rescigno, The gut-liver axis in liver disease: pathophysiological basis for therapy, J. Hepatol. 72 (3) (2020) 558–577.
[12] G. Anand, A. Zarrinpar, R. Loomba, Targeting dysbiosis for the treatment of liver disease, Semin. Liver Dis. 36 (1) (2016) 37–47.
[13] J. Fang, C.H. Yu, X.J. Li, J.M. Yao, Z.Y. Fang, S.H. Yoon, W.Y. Yu, Gut dysbiosis in nonalcoholic fatty liver disease: pathogenesis, diagnosis, and therapeutic implications, Front. Cell. Infect. Microbiol. 12 (2022) 997018.
[14] M. Zhou, J. Lv, X. Chen, Y. Shi, G. Chao, S. Zhang, From gut to liver: exploring the crosstalk between gut-liver axis and oxidative stress in metabolic dysfunction-associated steatotic liver disease, Ann. Hepatol. 30 (1) (2025) 101777.
[15] N. Li, L. Hao, S. Li, J. Deng, F. Yu, J. Zhang, A. Nie, X. Hu, The NRF-2/HO-1 signaling pathway: a promising therapeutic target for Metabolic dysfunction-associated steatotic liver disease, J. Inflamm. Res. 17 (2024) 8061–8083.
[16] X. Xu, K.L. Poulsen, L. Wu, S. Liu, T. Miyata, Q. Song, Q. Wei, C. Zhao, C. Lin, J. Yang, Targeted therapeutics and novel signaling pathways in non-alcohol-associated fatty liver/steatohepatitis (NAFL/NASH), Signal Transduct Target Ther 7 (1) (2022) 287.
[17] B. Bathish, H. Robertson, J.F. Dillon, A.T. Dinkova-Kostova, J.D. Hayes, Nonalcoholic steatohepatitis and mechanisms by which it is ameliorated by activation of the CNC-bZIP transcription factor Nrf2, Free Radic. Biol. Med. 188 (2022) 221–261.
[18] J. Zhou, Q. Zheng, Z. Chen, The Nrf2 pathway in liver diseases, Front. Cell Dev. Biol. 10 (2022) 826204.
[19] M.L. Steele, S. Fuller, M. Patel, C. Kersaitis, L. Ooi, G. Munch, Effect of Nrf2 activators on release of glutathione, cysteinylglycine and homocysteine by human U373 astroglial cells, Redox Biol. 1 (1) (2013) 441–445.
[20] G. Wu, Y.Z. Fang, S. Yang, J.R. Lupton, N.D. Turner, Glutathione metabolism and its implications for health, J. Nutr. 134 (3) (2004) 489–492.
[21] A. Hoffmann, P. Kleniewska, R. Pawliczak, Antioxidative activity of probiotics, Arch. Med. Sci. 17 (3) (2021) 792–804.
[22] O.V. Averina, E.U. Poluektova, M.V. Marsova, V.N. Danilenko, Biomarkers and utility of the antioxidant potential of probiotic Lactobacilli and Bifidobacteria as representatives of the Human Gut Microbiota, Biomedicines 9 (10) (2021).
[23] T. Kullisaar, E. Songisepp, M. Aunapuu, K. Kilk, A. Arend, M. Mikelsaar, A. Rehema, M. Zilmer, Complete glutathione system in probiotic Lactobacillus fermentum ME-3, Prikl. Biokhim. Mikrobiol. 46 (5) (2010) 527–531.
[24] H. Jang, H. Joung, J. Chu, M. Cho, Y.W. Kim, K.H. Kim, C.H. Shin, J. Lee, J.H. Ha, Lactobacillus delbrueckii subsp. lactis CKDB001 ameliorates metabolic complications in high-fat diet-induced Obese mice, Nutrients 16 (24) (2024).
[25] M. Cho, H. Joung, H. Jang, Y.W. Kim, J. Chu, Y.J. Kwon, C.H. Shin, J.H. Ha, J. Lee, Lactobacillus Plantarum Q180 Attenuates hepatic lipid accumulation and regulates energy metabolism in high-fat diet-induced Obese mice, Probiotics Antimicrob. Proteins (2026).
[26] D.H. Lee, J.S. Park, Y.S. Lee, J. Han, D.K. Lee, S.W. Kwon, D.H. Han, Y.H. Lee, S. H. Bae, SQSTM1/p62 activates NFE2L2/NRF2 via ULK1-mediated autophagic KEAP1 degradation and protects mouse liver from lipotoxicity, Autophagy (2020) 1–25.
[27] J.S. Park, D.H. Lee, Y.S. Lee, E. Oh, K.H. Bae, K.J. Oh, H. Kim, S.H. Bae, Dual roles of ULK1 (unc-51 like autophagy activating kinase 1) in cytoprotection against lipotoxicity, Autophagy 16 (1) (2020) 86–105.
[28] A.H. Patel, D. Peddu, S. Amin, M.I. Elsaid, C.D. Minacapelli, T.M. Chandler, C. Catalano, V.K. Rustgi, Nonalcoholic fatty liver disease in Lean/Nonobese and Obese individuals: a comprehensive review on prevalence, pathogenesis, clinical outcomes, and treatment, J. Clin. Transl. Hepatol. 11 (2) (2023) 502–515.
[29] R. Kumar, S. Mohan, Non-alcoholic fatty liver disease in lean subjects: characteristics and implications, J. Clin. Transl. Hepatol. 5 (3) (2017) 216–223.
[30] G.R. Steinberg, A.C. Carpentier, D. Wang, MASH: the nexus of metabolism, inflammation, and fibrosis, J. Clin. Investig. 135 (18) (2025).
[31] H. Tilg, A.R. Moschen, Evolution of inflammation in nonalcoholic fatty liver disease: the multiple parallel hits hypothesis, Hepatology 52 (5) (2010) 1836–1846.
[32] D.H. Lee, J.J. Jee, Y.S. Lee, D.Y. Kim, J.Y. Bang, H.W. Lee, H. Koh, S.H. Bae, Fecal microbiota transplantation improves hepatic fibro-inflammation via regulating oxidative stress in experimental NASH, Dig. Liver Dis. 55 (11) (2023) 1521–1532.
[33] J. Stout, D. De Vos, B. Vergauwen, S.N. Savvides, Glutathione biosynthesis in bacteria by bifunctional GshF is driven by a modular structure featuring a novel hybrid ATP-grasp fold, J. Mol. Biol. 416 (4) (2012) 486–494.

[34] T. Nakatani, I. Ohtsu, G. Nonaka, N. Wiriyathanawudhiwong, S. Morigasaki, H. Takagi, Enhancement of thioredoxin/glutaredoxin-mediated L-cysteine synthesis from S-sulfocysteine increases L-cysteine production in Escherichia coli, Microb. Cell Fact. 11 (2012) 62.
[35] L.M. Serrano, D. Molenaar, M. Wels, B. Teusink, P.A. Bron, W.M. de Vos, E.J. Smid, Thioredoxin reductase is a key factor in the oxidative stress response of Lactobacillus plantarum WCFS1, Microb. Cell Fact. 6 (2007) 29.
[36] M. Rojo de la Vega, D.D. Zhang, NRF2 induction for NASH treatment: a new hope rises, Cell. Mol. Gastroenterol. Hepatol. 5 (3) (2018) 422–423.
[37] A. Hammoutene, S. Laouirem, M. Albuquerque, N. Colnot, A. Brzustowski, D. Valla, N. Provost, P. Delerive, V. Paradis, Q.-N.R. Group, A new NRF2 activator for the treatment of human metabolic dysfunction-associated fatty liver disease, JHEP Rep. 5 (10) (2023) 100845.
[38] D.H. Lee, D.H. Han, K.T. Nam, J.S. Park, S.H. Kim, M. Lee, G. Kim, B.S. Min, B. S. Cha, Y.S. Lee, S.H. Sung, H. Jeong, H.W. Ji, M.J. Lee, J.S. Lee, H.Y. Lee, Y. Chun, J. Kim, M. Komatsu, Y.H. Lee, S.H. Bae, Ezetimibe, an NPC1L1 inhibitor, is a potent Nrf2 activator that protects mice from diet-induced nonalcoholic steatohepatitis, Free Radic. Biol. Med. 99 (2016) 520–532.
[39] V.F. Rodrigues, J. Elias-Oliveira, I.S. Pereira, J.A. Pereira, S.C. Barbosa, M.S. G. Machado, D. Carlos, Akkermansia muciniphila and gut immune System: a good friendship that Attenuates inflammatory bowel disease, obesity, and diabetes, Front. Immunol. 13 (2022) 934695.
[40] J. Liu, H. Qiu, J. Zhao, N. Shao, C. Chen, Z. He, X. Zhao, J. Zhao, Y. Zhou, L. Xu, Parabacteroides as a promising target for disease intervention: current stage and pending issues, npj Biofilms Microbiomes 11 (1) (2025) 137.
[41] J.S. Kim, K.C. Lee, M.K. Suh, K.I. Han, M.K. Eom, J.H. Lee, S.H. Park, S.W. Kang, J. E. Park, B.S. Oh, S.Y. Yu, S.H. Choi, D.H. Lee, H. Yoon, B.Y. Kim, S.J. Yang, J.S. Lee, Mediterraneibacter butyricigenes sp. Nov., a butyrate-producing bacterium isolated from human faeces, J. Microbiol. 57 (1) (2019) 38–44.
[42] C.H. Ng, W.H. Lim, G.E. Hui Lim, D.J. Hao Tan, N. Syn, M.D. Muthiah, D.Q. Huang, R. Loomba, Mortality outcomes by fibrosis stage in Nonalcoholic Fatty liver disease: a systematic review and meta-analysis, Clin. Gastroenterol. Hepatol. 21 (4) (2023) 931–939 e5.